UNIVERSITY OF CALIFORNIA

Los Angeles

Magnetic Signatures at Asteroid Flybys:
Locally Generated or Accidental?

A thesis submitted in partial satisfaction of the
requirements for the degree Master of Science
in Geophysics and Space Physics

by

Steven Peter Joy

1997

The thesis of Steven Peter Joy is approved.

_____

Christopher T. Russell

_____

Raymond J. Walker

_____

Margaret G. Kivelson, Committee Chair

University of California, Los Angeles

1997

Dedication

I dedicate this thesis to my loving wife Ella, my children David and Danielle, and my father Joseph Joy. Without the love and support of Ella, this work would never have been possible. She raised our children and provided me with emotional support throughout my graduate career. My children missed having a father at home for much of their formative years. This is something I can never replace and I hope in the end their sacrifice was justified. My father has always been a driving force in my life. He has always believed in my ability to succeed, academically and otherwise, even when I questioned myself. I love you all. Thanks for your love and support...

<u>Contents</u>

List of Figures

List of Tables

List of Acronyms

AU: Astronomical Unit: Equivalent to the mean distance between the Sun and the Earth.

DD: Directional Discontinuity

EMHD: Electron Magnetohydrodynamics, an approximation to plasma equations that assumes that the ion density and velocity are constant and that charge neutrality is maintained. No further assumptions are made about the electron mass, density, or velocity.

Hall MHD: An approximation to the plasma equations that electrons are magnetized so that $\mathbf{E} = -\mathbf{v_e} \times \mathbf{B}$ but that ions are not. Ion velocity must satisfy $\mathbf{j} = ne(\mathbf{v_i} - \mathbf{v_e}) = \frac{1}{\mu_o}(\nabla \times \mathbf{B})$.

IMF: Interplanetary Magnetic Field

I.G.P.P.: Institute of Geophysics and Planetary Physics

LB: Lepping and Behannon (1986) DD selection criteria.

MHD: Magnetohydrodynamic. A set of approximations to Maxwell's equations and the fluid equations used to describe a plasma as a fluid rather than as a collection of particles. It assumes time scales that are long compared to microscopic particle motions and spatial scales large compared to the thermal particle gyroradius.

NSSDC: National Space Science Data Center

RD: Rotational Discontinuity

ROID: Rate of Occurrence of Interplanetary Discontinuities

RTN: A coordinate system commonly used for IMF data. The RTN (Radial-Tangential-Normal) coordinate system has the R vector radial out from the center of the Sun in the direction of the spacecraft, the T direction is perpendicular to R and parallel to the equatorial plane of the Sun, positive in the sense of planetary orbital motion, and N completes the right-handed set.

TD: Tangential Discontinuity

TS: Tsurutani and Smith (1979) DD selection criteria

Acknowledgments

ABSTRACT OF THE THESIS

Magnetic Signatures at Asteroid Flybys:
Locally Generated or Accidental?
by
Steven Peter Joy
Master of Science in Geophysics and Space Physics
University of California, Los Angeles, 1997
Professor Margaret G. Kivelson, Chair

The Galileo spacecraft observed two asteroids, 951 Gaspra and 243 Ida, during its cruise to Jupiter. At each of these asteroid encounters, magnetic field rotations were recorded as the spacecraft approached the interplanetary magnetic field (IMF) line connecting the spacecraft and asteroid. Kivelson et al. (1993; 1995) interpret these field rotations as evidence that the solar wind plasma interacts with magnetized asteroids to produce standing whistler wave wakes. An upper limit is set on the likelihood that magnetic observations during the asteroid flybys were random fluctuations in the IMF by using data from the Ulysses magnetometer acquired during its asteroid belt crossing. Ulysses did not come close to any asteroids. Criteria are developed that identify IMF structures with characteristics similar to those observed during the asteroid encounters. The event selection criteria identify 8.96 ± 1.23 asteroid-like events per day. The mean event separation time (161 ± 22 minutes) and standard deviation (233 minutes) are inconsistent with a Poisson distribution where these two moments should be equal. A lognormal probability density function is used to compute probabilities. The Galileo magnetometer recorded an event satisfying the selection criteria in the central 15 minutes of a two hour observation and no other events were observed. The likelihood of observing an isolated event similar to the Galileo observations is less than 5% and probably on the order of 1%. We conclude that the magnetic field rotations observed at Gaspra are not random fluctuations of the IMF.

1 Introduction

Several spacecraft have passed through the asteroid belt during their flight to the outer planets but the Galileo spacecraft was the first spacecraft to specifically target an asteroid for scientific observation. Galileo observed two asteroids, 951 Gaspra and 243 Ida, during its journey to Jupiter. A wealth of new data on the shape, age, composition, and orbital properties of these asteroids were obtained during these flybys. While Galileo was acquiring information about the geology of the asteroids, the fields and particles experiments aboard the spacecraft were also collecting data. The magnetometer data acquired in the vicinity of both of these asteroids showed field rotations at the time when the spacecraft approached the interplanetary magnetic field (IMF) line connecting the spacecraft and asteroid. A few minutes later, the IMF rotated back to its initial orientation suggesting an interaction with the asteroid. The IMF is known to have fluctuations on many temporal and spatial scale sizes. This study examines the likelihood that the rotations observed in the Galileo magnetometer data during the asteroid flybys are random events in the solar wind unrelated to the presence of a nearby asteroid.

The solar wind and the interplanetary magnetic field (IMF) have been observed by numerous spacecraft. The solar wind contains numerous irregularities. Structures that are separated by an abrupt change in the plasma or IMF conditions are called discontinuities. Discontinuities are further classified as rotational, tangential or contact discontinuities, or as shock waves, according to the exact nature of the changes that occur (Burgess, 1995). Solar wind discontinuities have been extensively studied over the last 30 years. Variations in their rate of occurrence (Burlaga, 1968; Mariani et al., 1973; Tsurutani and Smith, 1979; Lepping and Behannon, 1986), their origin, evolution, and characteristic scale sizes (Siscoe et al., 1968; Neugebauer and Buti, 1990; Neugebauer and Alexander, 1991; Neugebauer et al., 1993; Kraus-Varban, 1993; Tsurutani et al., 1994), and the relative abundance of the various types of discontinuities (Burlaga et al., 1977; Neugebauer et al., 1984; Lepping and Behannon, 1986) have all been studied.

Here we examine a particular aspect of the IMF variability that has not been previously studied: How common are small scale discontinuities in the interplanetary magnetic field at a distance of 2-3 AU from the Sun in the ecliptic plane? Small scale structures are roughly defined as structures that affect the prevailing IMF direction for time intervals of the order of tens of minutes or less, or conversely, over small spatial scales. The discussion of exactly what is meant by small temporal or spatial sizes is deferred until later.

The problem of small scale structures is of interest in relation to magnetic field rotations observed in the neighborhood of asteroids. These rotations have been attributed to a solar wind – asteroid interaction (Kivelson et al., 1993; Kivelson et al., 1995; Wang and Kivelson, 1996). The solar wind interaction with any object is expected to have a spatial scale that is proportional to the size of the object. If the object is small, like an asteroid, comet, or small moon, then the

signature of the interaction with the solar wind will last only briefly as an observing spacecraft quickly passes the object of interest. However, a brief disturbance in the IMF could be unrelated to the presence of a small body near the spacecraft. Therefore, if a fluctuation of the IMF is observed, the question must be asked: how likely is it that the observed signature is unrelated to the body of interest, that it is just a random fluctuation of the solar wind? In order to answer this question, this study examines the rate of occurrence of small scale rotational structures in the IMF in the vicinity of the asteroid belt far from any known asteroids. This work sets an upper limit on the rate of occurrence of solar wind structures similar to those observed during the Galileo asteroid flybys in the absence of an asteroid interaction. At the same time, a lower limit estimate of the probability that the observed Galileo magnetometer signatures are random solar wind fluctuations is determined.

1.1 Asteroid Observations

Galileo targeted two S-type asteroids for observation during its excursions into the asteroid belt, Gaspra and Ida. Gaspra is a small oblong body approximately 7 kilometers in average radius (Belton et al., 1992) located near the inner edge of the asteroid belt (2.2 AU). Galileo made its closest approach to Gaspra on October 29, 1991 at 22:36:40 UT at a range of 1600 kilometers. The spacecraft passed the asteroid on its dawn side slightly above the plane of Gaspra's orbit about the Sun (Figure 1.1). Ida is a slightly larger, highly elongated, asteroid with an average radius of about 15.7 kilometers (Belton et al., 1995). Ida is located in the central asteroid belt at a heliocentric distance of 2.9 AU. The spacecraft passed by Ida slightly on the dawn side of the asteroid but primarily below the plane of its orbit (Figure 1.2). Closest approach to Ida was on August 28, 1993 at 16:52:01 UT at a range of 2407 kilometers.

The Galileo fields and particles experimenters did not expect to observe an interaction between Gaspra and the solar wind because of the large closest approach distance ($\approx$225 Gaspra radii) and small asteroid size ($\approx$7 km). However, spacecraft resources were available to make Gaspra observations, so about two hours of high rate fields and particles data, roughly centered at closest approach, were recorded to tape. These data were then played back when the spacecraft returned to Earth for its second Earth flyby. In addition, the magnetometer acquired low resolution averages ($\sim$16-64 minute) of the magnetic field before and after the encounter in order to characterize the large scale solar wind configuration at the time of the encounter. Figure 1.3 shows the magnetic field data acquired for roughly three solar rotations that include the Gaspra encounter. The interplanetary magnetic field (IMF) exhibits the simple two sector structure expected for this phase of the solar cycle and heliospheric latitude (Smith, 1989) with field compressions at the sector boundaries. As indicated by the vertical line in the figure, the Gaspra encounter occurred in the quiet IMF about 12 hours before a sector crossing and associated field compression.

Figure 1.1 (revised from Kivelson et al., 1993, Figure 2) Projections of the magnetic field vectors plotted at 4 second intervals along the trajectory of the spacecraft in Gaspra IMF coordinates (X along Gaspra-Sun line, the average IMF from 22:30 – 22:32 UT [B_0 = (0.1, 1.6, 0.5)] in nanoTesla lies in the X-Y plane, Z completes the right-handed set). The thickened portion of the trajectory indicates the asteroid interaction region. Figure 1a shows the magnetic field vectors of the solar wind IMF rotate from their upstream orientation into a new orientation that is consistent with field line draping around the asteroid. Figure 1b shows the X-Z plane projection of the flyby where field draping is also apparent.

A

Gaspra

Sun

Y

22:40

22:35

Closest Approach
22:36:40

B

22:35

Z

22:40

1000 km

Gaspra

2 nT

UCLA
MAG

X

Gaspra not to scale.

3
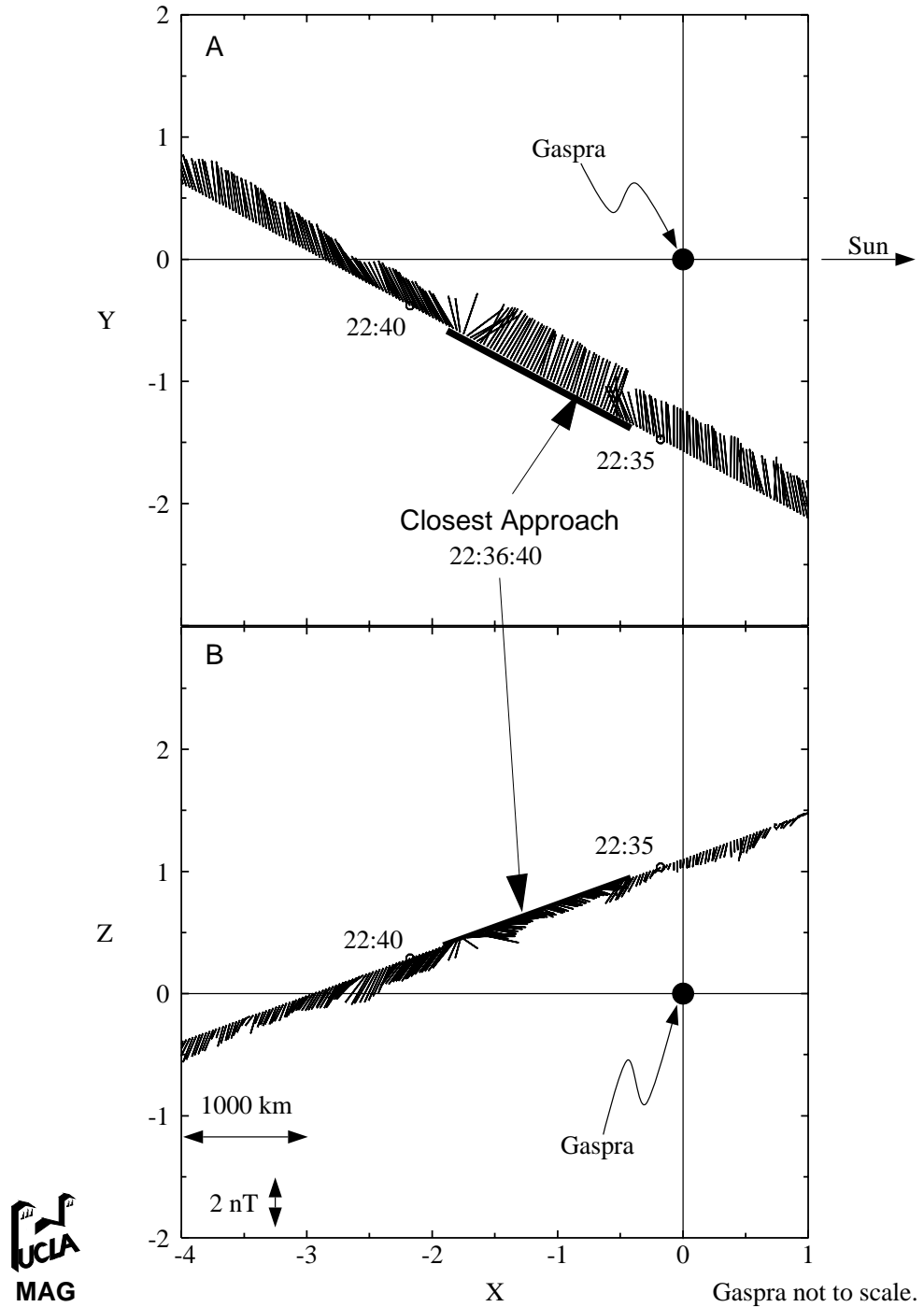
Figure 1.2 Trajectory of Galileo past the asteroid Ida in Ida IMF coordinates (X along Ida-Sun line, positive towards the Sun, the average IMF from 16:40 - 16:45 UT [B_0 = (-2.1, 3.4, -0.7)] in nanoTesla lies in the X-Y plane, Z completes the right-handed set). The thickened line of trajectory indicates the asteroid interaction region. 1a shows the X-Y plane projection of the trajectory. 1b shows the X-Z plane projection of the flyby. Note that the onset of the interaction begins upstream (positive X) of Ida at 16:46 UT. and that no draping of the IMF is observed as the spacecraft passes the asteroid.
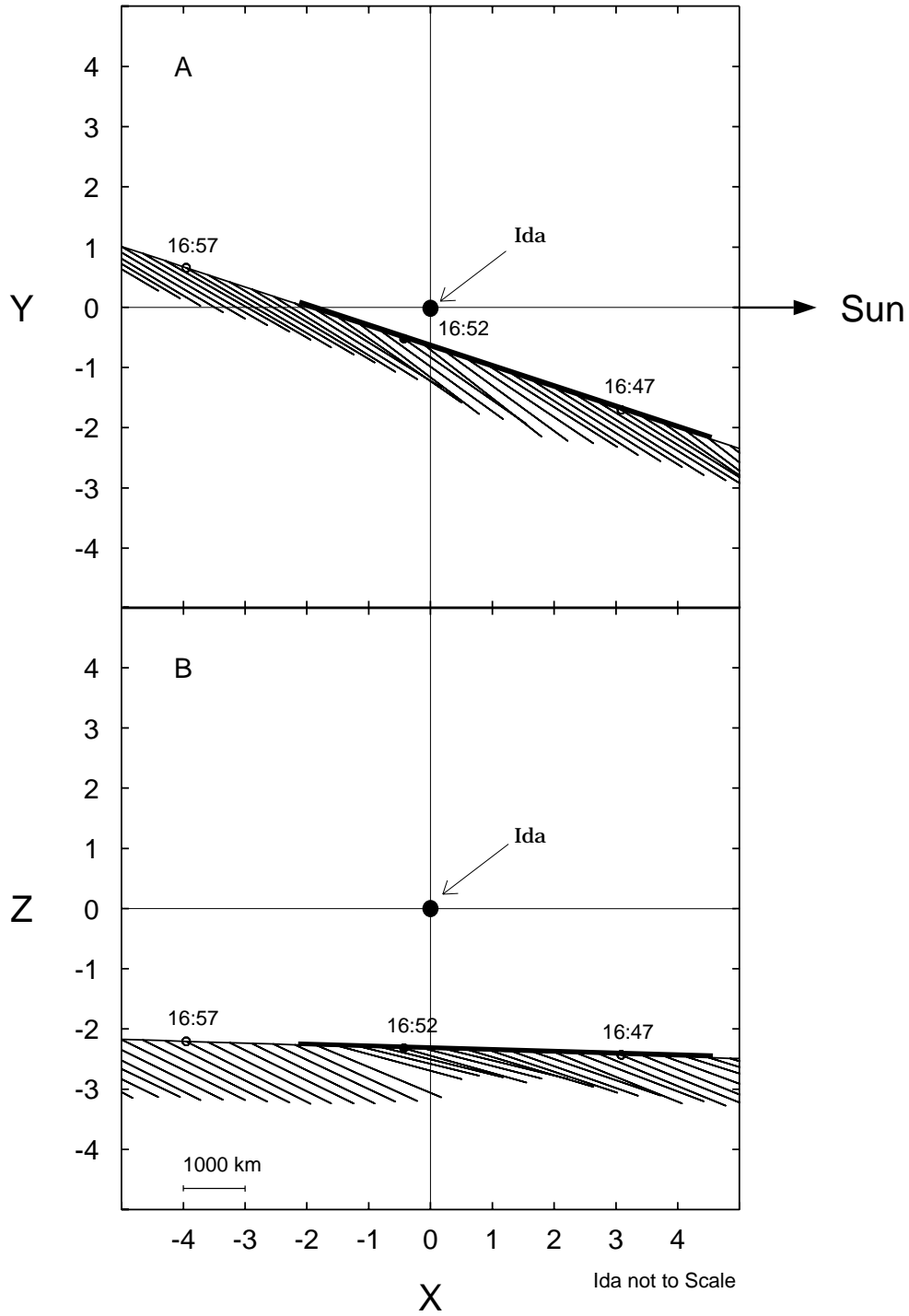
Figure 1.4 shows the observed magnetic field vectors (10 second averages) for the two hours of high rate data in radial-tangential-normal (RTN) coordinates.[1] The field magnitude is steady at about 2 nT. As the spacecraft passed by the asteroid Gaspra, the magnetometer measured a pair of sharp field rotations, primarily in the B_R component. During this rotation pair, the field rotates sharply just before closest approach (22:37) and then returns to the unperturbed direction after a few minutes. There are several other field rotations in this interval where the field does not return to an initial orientation (21:52, 22:18, 23:01) after a short interval. These other rotations are the sort of events commonly identified as rotational discontinuities. The paired rotations near closest Gaspra approach are typically not counted as rotational discontinuities; "box-car-like" and "wave-like" structures are explicitly excluded from studies of solar wind discontinuities (Mariani et al., 1973; Tsurutani and Smith, 1979; Lepping and Behannon, 1986).

---

[1]   The RTN coordinate system is defined as follows: The R (radial) direction lies along the line between the Sun and the spacecraft, positive away from the Sun. The T (tangential) direction is perpendicular to R and parallel to the solar equatorial plane. The N (normal) direction completes the right-handed set (N = R x T)

Figure 1.3 Low resolution data from the Galileo Magnetometer optimal averager. Ninety days of data that include the Gaspra flyby are shown in RTN coordinates (see text). Gaspra closest approach is indicated by the solid vertical line. The two sector structure is identified by shading the "toward" sectors and leaving the "away" sectors unshaded. Note that there are field compressions spanning the sector boundaries.

Figure 1.4 This plot identifies the high resolution data acquisition interval around the Gaspra flyby by using 10 second averages of the magnetic field data in RTN coordinates. The vertical line marks the Gaspra closest approach and the shaded region shows the time interval that has been interpreted by Kivelson et al. (1993) as the asteroid interaction region.
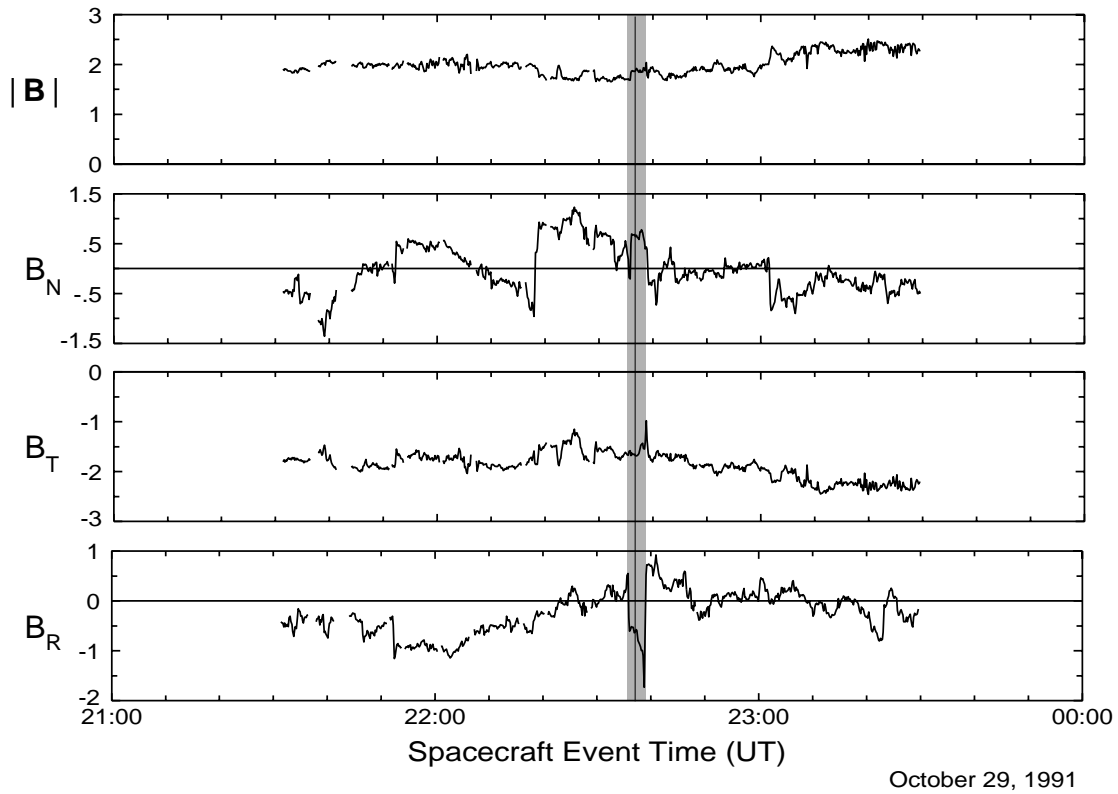
The interval between 22:30 and 22:45 UT has been expanded in Figure 1.5 to show the details of the magnetic field observed during the asteroid flyby. During the interval from 22:30 to 22:34 UT the magnetic field was nearly constant. The dashed line shows the average upstream field direction ($B_R = 0.126, B_T = -1.60, B_N = 0.496$ in nT). The panel labeled θ shows the angle the instantaneous field vector makes relative to this upstream field vector. Just prior to the first large rotation defining the asteroid interaction region ($\sim$22:35 UT), there is a small rotation of the field that brings the field to an orientation of ($B_R = 0.56$, $B_T = -1.52$, $B_N = -0.21$).

Figure 1.5 Full resolution (2/9 sec) Galileo Magnetometer data for the Gaspra flyby in RTN coordinates. The vertical line shows the time of Gaspra closest approach and the shaded region again shows the asteroid interaction as identified by Kivelson et al. (1993). The dashed line in the panels containing magnetic field data is the average value of the upstream IMF during the interval between 22:30 and 22:32 UT. The top panel labeled θ shows the angle between field vectors and the upstream field orientation in degrees. θ is taken to be positive when $B_R \geq 0$ and negative when $B_R < 0$
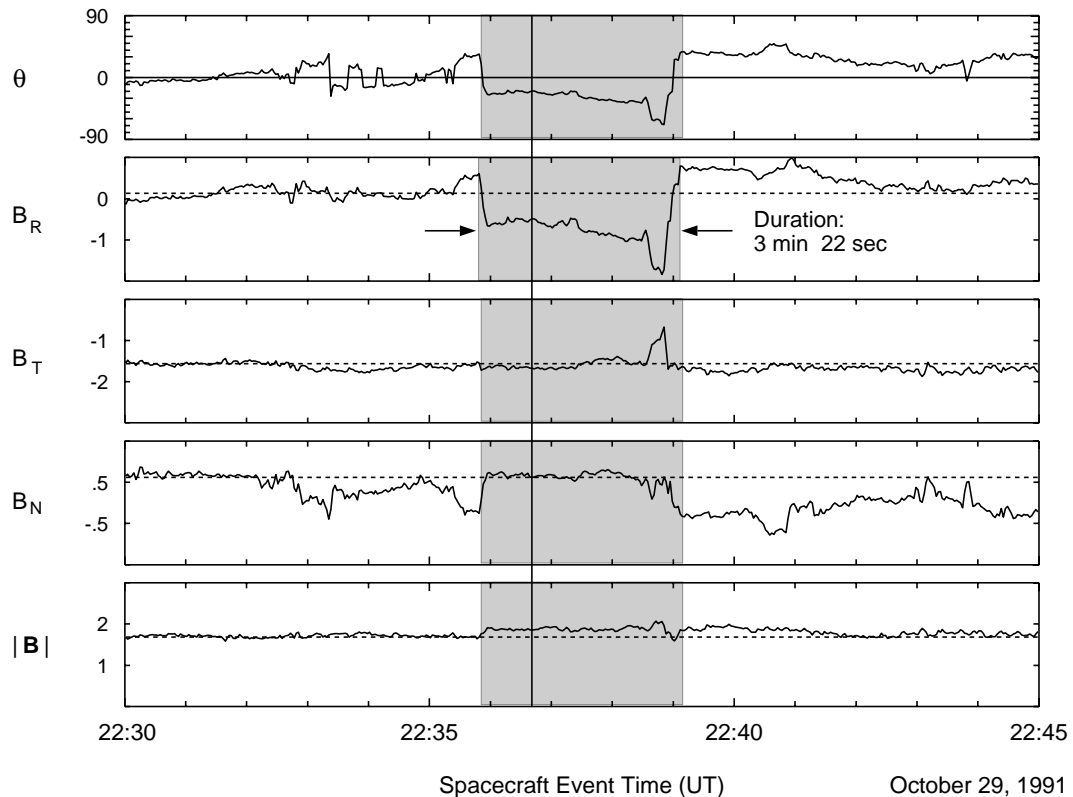
At 22:35:47 UT the field rotates $60°$ to (B_R = -0.67, B_T = -1.62, B_N = 0.69) and then at 22:39:07 the field rotates back to (B_R= 0.79, B_T = -1.66, B_N = -0.27), or nearly its orientation at 22:35 UT. During the second rotation, the field rotates through $104°$ in 16 seconds. The field remains in the perturbed orientation for 3 minutes and 22 seconds. There is no apparent wave activity visible in the data either inside or near boundaries of the interaction region. The change in field magnitude over the duration of the interaction is about 0.2 nT or 10% of the background field strength.

For the Ida flyby, the spacecraft tape recorder was not available to record data from the fields and particles investigations until one minute after the asteroid closest approach. In order for the magnetometer investigation to be able to acquire moderately high resolution data across the asteroid passage, the instrument had to be operated in a new manner. The data were acquired in the optimal averager mode of the instrument (Kivelson et al., 1992) and sampled by the spacecraft every 4/3 second. Unfortunately, the optimal averager (low pass filter) mode of the instrument was set to highly filter the data prior to sampling it.[2] Although the Galileo Magnetometer team

---

[2]   The optimal averager mode of the Galileo magnetometer employs a recursive filter and decimate procedure. The filter recursion constant and decimation factor are ground commandable to generate samples of various averaging lengths. At Ida, the filter parameter was set to take 1 minute averages, its highest rate. Using this filter parameter, the filter corner frequency is 1/137 Hz. A detailed discussion of the optimal averager and its usage can be found in Kivelson et al. (1992)
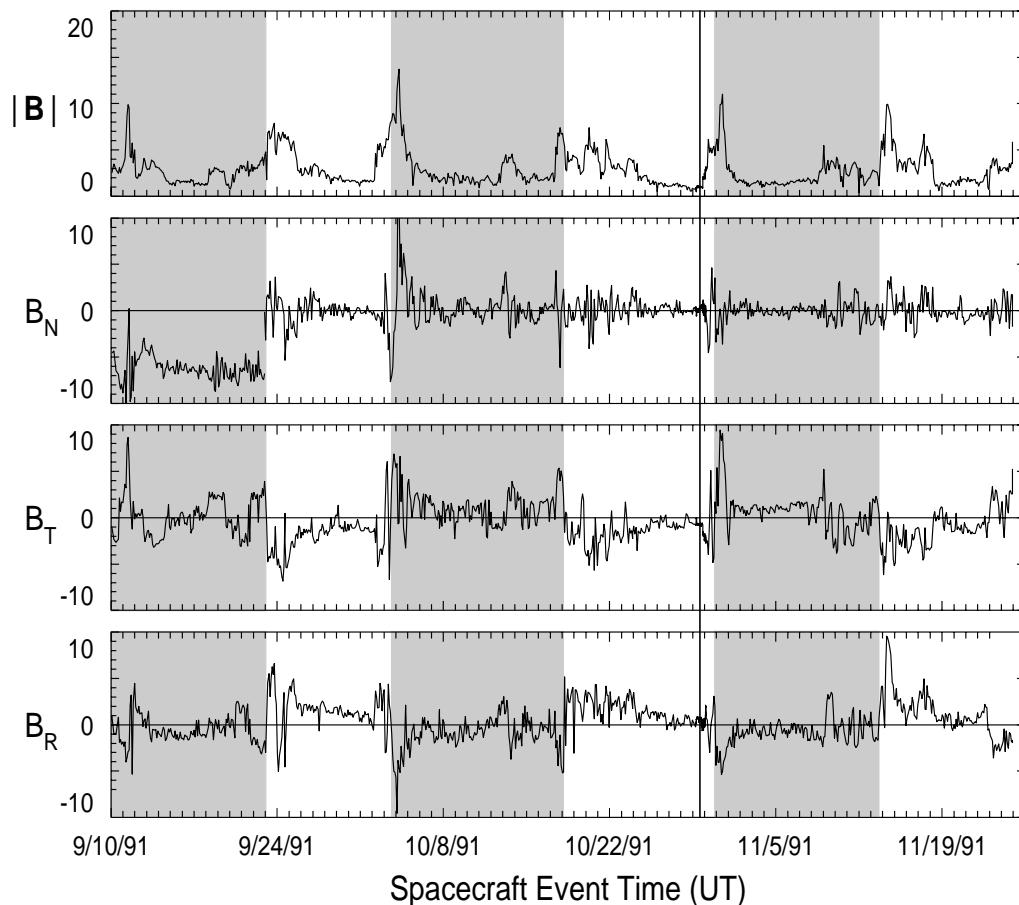
Figure 1.6 Low resolution data from the Galileo Magnetometer optimal averager. Ninety days of data including the Ida flyby are shown in RTN coordinates. Ida closest approach is marked with a vertical line. Note that the field strength enhancements appear at regular intervals suggesting that they are related to persistent solar structures. Large data gaps are the result of malfunctions associated with the spacecraft power system.
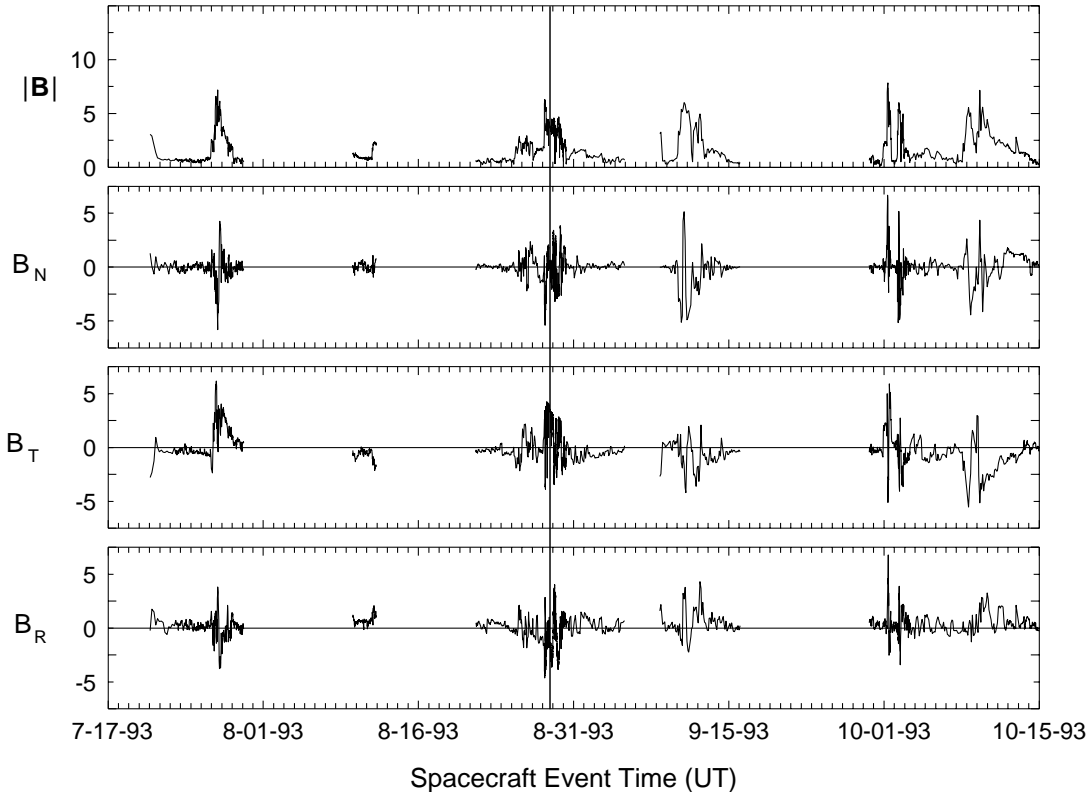
put considerable effort into recovering the full amplitude and frequency content of the 4/3 second data, it is likely that the data do not contain the same high frequency content as the original data. It is possible that the inferred signature of Ida might be more distinct (abrupt) than it appears in the heavily low pass filtered dataset.

Figure 1.6 shows the data for roughly 3 solar rotations centered on the Ida flyby. The data are quite sparse. During the months both before and after the Ida flyby, the spacecraft was experiencing power problems that may have been associated with dust particles in the spin-bearing assembly. Every time these power problems occurred, the spacecraft turned off the magnetometer experiment. It is difficult to see any clear-cut sector structure or boundaries in these data. However, regions of enhanced field strength similar to the compression observed at the sector boundaries during the Gaspra epoch are clearly visible in the data. Furthermore, the Ida flyby is near the center of one of these regions of enhanced field strength.

Fortunately, the data stream was fairly continuous for the two weeks centered on the Ida encounter. Figure 1.7 shows the high resolution data (RTN coordinates) acquired by the

Figure 1.7 This figure shows the high resolution data acquisition interval for the Ida flyby by using 10 second averages of the field in RTN coordinates. The vertical line shows the time of Ida closest approach. As in the Gaspra plots, the shaded region shows the time interval that has been interpreted by Kivelson et al. (1995) as the asteroid interaction region. The steady decrease in the B_N and B_T components between 16:00 and 17:30 UT indicates a change in the background field orientation over the observation. The field magnitude remained constant during the field reorientation.
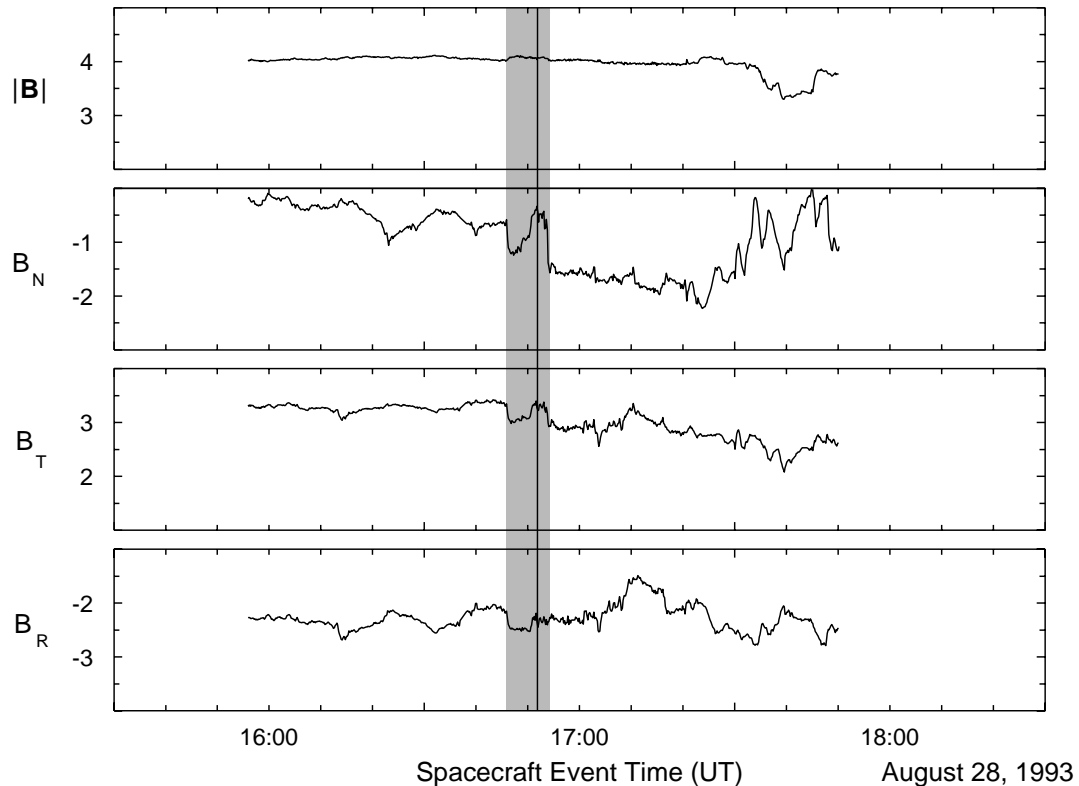
magnetometer in optimal averager mode for the two hours that contain the asteroid encounter. The data shown have been averaged to 10 second samples. The shaded region shows the data interval that Kivelson et al. (1995) interpret as an asteroid interaction region. The solid vertical line indicates the time of Ida closest approach. For most the interval the field magnitude is very steady at about 4 nT. However, the individual field components are not constant. In particular, the B_n appears to be steadily decreasing (becoming more negative) between 16:00 and 17:30 UT. At the end of the data interval, beginning at about 17:30, the field is disturbed by wave-like structures predominantly in the B_N component. The field magnitude drops slightly during the disturbed interval.

The 20 minute interval center at 16:50 UT shows the details of the solar wind magnetic field that may be interacting with the asteroid Ida (Figure 1.8). Once again the data are presented in RTN coordinates, this time at the full 4/3 second sample rate. Shading again highlights the interaction region and the vertical line indicates the time of closest approach at 16:52:01 UT. The field rotates from its upstream orientation by 8° beginning at 16:46:04 UT. Over the next eight minutes the field slowly rotates in a roughly sinusoidal pattern. At 16:54:06 UT the field rotates back 16° to a orientation that is consistent with the gradual change previously described over the interval between 16:00 and 17:30 UT.

9

Figure 1.8 Full resolution (4/3 sec) magnetic field data for the Ida flyby in RTN coordinates. The vertical line marks the time of Ida closest approach (2407 km, 16:52:01 UT) and the shaded region again shows the asteroid interaction region as identified by Kivelson et al. (1995). The dashed lines are the average upstream field component values evaluated over the interval between 16:40 and 16:45 UT and θ is the angle between the instantaneous field direction and the upstream field direction. Comparison with Figure 1.5 shows that the apparent frequency content of these data is much less than would be expected for data sampled every 4/3 second.
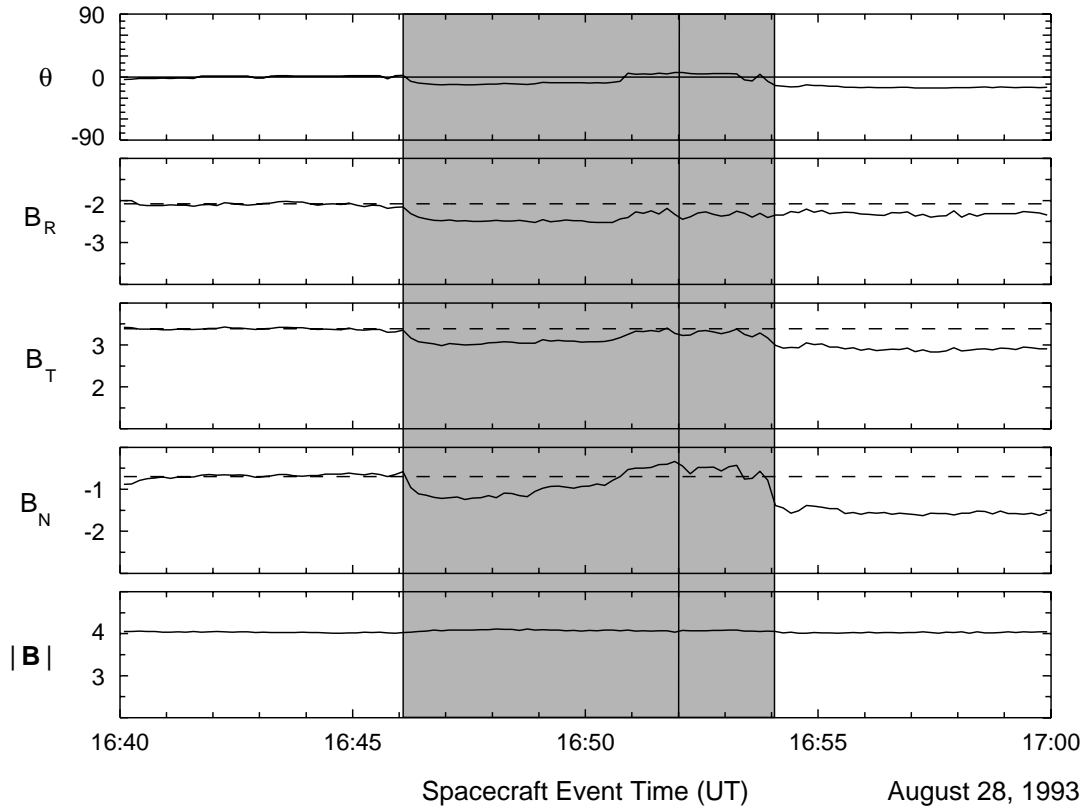
The magnetic signature observed during the Ida flyby is far less dramatic than the one observed during the Gaspra flyby. There are many factors which collectively may help to explain the weakness of the signature. First, the Ida flyby took place at an approach distance of 2407 km which is one third greater than the distance of the Gaspra flyby (1600 km). Secondly, the onset of the observed signature occurred upstream of the asteroid. The detection upstream of the source can be understood for an interaction in the whistler mode. The whistler mode propagates in plasma rest frame, preferentially along $\pm\mathbf{B}$, at a speed greater than $\mathbf{V}_{sw}$ (Wang and Kivelson, 1996). Waves detected upstream will have traveled a greater distance than those detected downstream, an equal distance from the source. Wave dissipation should be greater in the upstream case. In addition, the Ida data were acquired using the optimal averager mode of the instrument. The data were over-filtered relative to their sampling frequency and the full filter response function may not have been recovered. And finally, and probably most importantly, the Ida flyby occurred in a region of enhanced IMF strength. The field magnitude during the Ida flyby was more than double the field strength at Gaspra. The size of the change in the dominant components at the bounding rotations at Ida (1.1 nT in B_N) are similar to those observed at

Gaspra (1.25 nT in B_R). However at Ida the rotation angle was much smaller ($16°$ versus $104°$), because the field magnitude was larger.

In summary, both asteroid observations are characterized by field rotations with little or no change in the field magnitude. After a short time interval, the field rotates back to an orientation that is consistent with the long period changes that are occurring in the background field. In addition to the field not changing magnitude at the bounding rotations, there is very little change in field magnitude over the entire duration of the signatures. At Gaspra, the signature has a "boxcar" appearance and the field remains in its perturbed orientation for a little more than three minutes. The bounding rotations are quite sharp; the field rotates more than $104°$ in 16 seconds ($> 6°$/sec). At Ida, the signature is much weaker and has a "down-up-down" or square-wave appearance. The duration of the Ida signature is about eight minutes where the duration of the signature is defined as the time it takes the solar wind to rotate back to its unperturbed orientation after the initial rotation. The bounding rotations are not nearly as sharp as those observed during the Gaspra flyby. The field rotates only $16°$ over 11 seconds or $1.5°$/sec. In addition, there is no wave activity apparent either during the signatures or in the immediate vicinity of the signatures.

1.2 Asteroid Interactions with the Solar Wind: Supporting Theory

Eugene Greenstadt first postulated that there could be an observable magnetic interaction between the solar wind and small bodies of asteroid sizes (Greenstadt, 1971a). Using calculations based on average solar wind properties at 2.8 AU and observed magetizations in meteorites and in lunar rocks, Greenstadt computed the solar wind stand-off distance (magnetopause location). Greenstadt also understood that there might be an observable interaction that would fall into the whistler wave branch of the plasma dispersion relation (Greenstadt, 1971a, 1971b). Whistler waves are generated when the scale size of the interacting body is intermediate between the Larmor radii of electrons and protons ($\rho_c = mv_\perp/qB$). For typical solar wind conditions $B \approx 3$ nT, $V_\perp \approx 400$ km/sec, this gives $\rho_e \approx 1$ km and $\rho_i \approx 2000$ km where ρ_e and ρ_i are the electron and ion Larmor radii respectively. Greenstadt concluded that in order to directly observe an asteroid magnetosphere, the asteroid would have to be large (> 100 km) and the spacecraft would have to approach within 20–40 asteroid radii (Greenstadt, 1971b). However, Greenstadt (1971a, 1971b) did postulate that plasma waves and electrostatic noise generated by the interaction of the solar wind with a magnetospheric cavity might be detectable at much larger flyby distances.

Wang and Kivelson (1996) have recently published the results of their simulation of the solar wind interaction with a magnetized asteroid. In this work, the authors explore both the analytical and numerical solutions to the relevant plasma equations (electron magnetohydrodynamic[3] (EMHD) and Hall MHD[4]) for conditions which approximate the solar wind conditions at the time of the Galileo flybys of the asteroids Gaspra and Ida. The small scale lengths of the asteroids places any resulting interaction along the whistler waves branch of the warm plasma dispersion relation. However, the relatively large area of the asteroid disturbances suggests that the effective scale size the asteroids is substantially larger than the asteroids themselves. Kivelson and Wang (1996) postulate that the asteroids are weakly magnetized, allowing them to have a larger effective scale size in the magnetized plasma of the solar wind. This effective scale size is on the order of a 1–2 hundred, rather than 7–15, kilometers. This larger effective scale size is still far below the wavelength of MHD waves. The interaction between the solar wind and a magnetized asteroid takes the form of a whistler mode mediated standing wave, or whistler wake (Wang and Kivelson, 1996). A magnetized asteroid is required to produce the standing whistler wake in the Wang and Kivelson simulations in a self-consistent manner (Wang et al., 1995).

The dispersive nature of the whistler wave makes the whistler wake more similar to a ship's bow wake than a standard MHD wake (Wang and Kivelson, 1996). The dispersion relation for deep water is $\omega \propto \sqrt{k}$ and the bow wake has the familiar form which is convex away from the ship. In the simplest of geometries where the magnetic field is perpendicular to the plasma flow, the whistler wave dispersion relation has the form $\omega \propto k^2$ (Wang and Kivelson, 1996). The shape of this wake is parabolic, concave towards the obstacle, opposite that of a ship wake (see Figure 1.9). Figure 1.9 shows the wake wave in the EMHD regime which is composed of a series of 180° rotations in the transverse components of the field (Wang and Kivelson, 1996). The component of the field normal to the wave fronts, and the field magnitude, are mostly unchanged across wave fronts (Wang and Kivelson, 1996). The perturbation associated with a wave front crossing is similar to the field perturbations produced by the passing of an Alfvén wave or a rotational discontinuity in the solar wind (Alfvén, 1942)[5]. As the restrictions on the plasma flow and field orientations are relaxed, the shape of the whistler wake becomes more complex (Wang and Kivelson, 1996).

---

[3]   The electron MHD (EMHD) approximation assumes that ion density and velocity are constant and that charge neutrality is maintained. In this limit, electron motion is primarily governed by **ExB** drift and magnetic field perturbations are *frozen in* to the fluid electrons. The EMHD approximation is valid only for wavelengths greater than several electron Larmor radii and much smaller than the ion Larmor radii.

[4]   Hall MHD treats ions as fluid and adiabatic and electrons as frozen in to the magnetic field and massless. Conventional MHD has the field frozen in to the ions. The approximation works well for frequencies below the lower hybrid frequency where finite electron mass effects are small. (Wang and Kivelson, 1996)

[5]   Rotational discontinuities are sometimes referred to as "Alfvénic Shocks" since they are equivalent to a large-amplitude Alfvén wave propagating along the large-scale magnetic field (Burlaga,1995)

Figure 1.9 (from Wang and Kivelson, 1996) Schematic for the whistler wake wave for the Gaspra case ($\mathbf{V_{sw}} \perp \mathbf{B}$) The asteroid is at (0,0). The wake wave in the EMHD regime is composed of a series of magnetic rotations. Between each pair of parabolic lines, the transverse magnetic field rotates by $180°$. The EMHD regime is valid only between the fastest front and the Alfvén Mach cone.
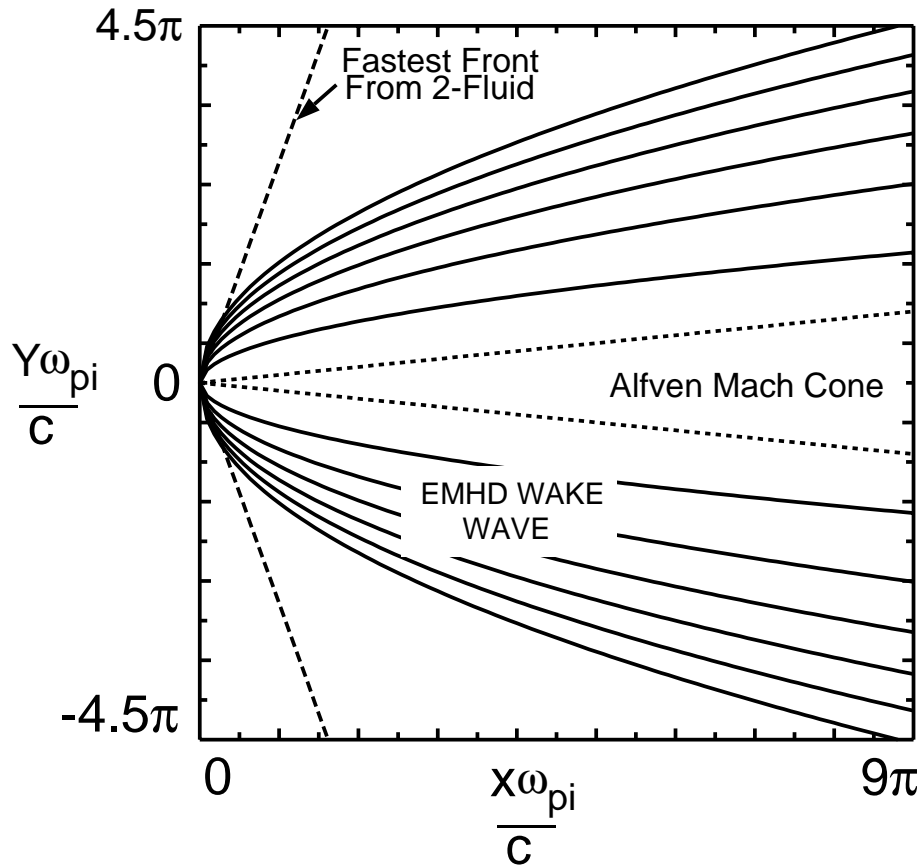
Figure 1.10 shows the whistler wave dispersion relation for hot and cold plasmas when the wave vector is parallel to the magnetic field (Wang and Kivelson, 1996). Short wavelengths propagate faster than longer wavelengths as indicated in the figure. Another property of whistler waves is that they propagate anisotropically, primarily along magnetic field lines. Figure 1.11 shows the Friedrichs diagrams (Kivelson et al., 1995) for both the group and phase velocities of whistler waves for both the full two-fluid and EMHD dispersion relations. The Friedrichs diagram shows that the group velocity is largest for propagation along the magnetic field. Whistler waves can have group velocities that are greater than the solar wind speed which allows them to propagate upstream of their source in the solar wind. Finite electron mass effects limit the wave speed to being less then 27.8 times the Alfvén speed V_A (Wang and Kivelson, 1996), however, this constraint does not prevent propagation upstream in the solar wind.

Figure 1.10 Whistler wave dispersion relation for both hot $B_e = 1$ and cold $B_e = 0$ plasma for wave propagation parallel to the magnetic field (Wang and Kivelson, 1996). The electron MHD and Hall MHD regions are indicated. In the EMHD region, the dispersion relation can be approximated by $\omega = \alpha k_z{}^2$ for parallel propagation.
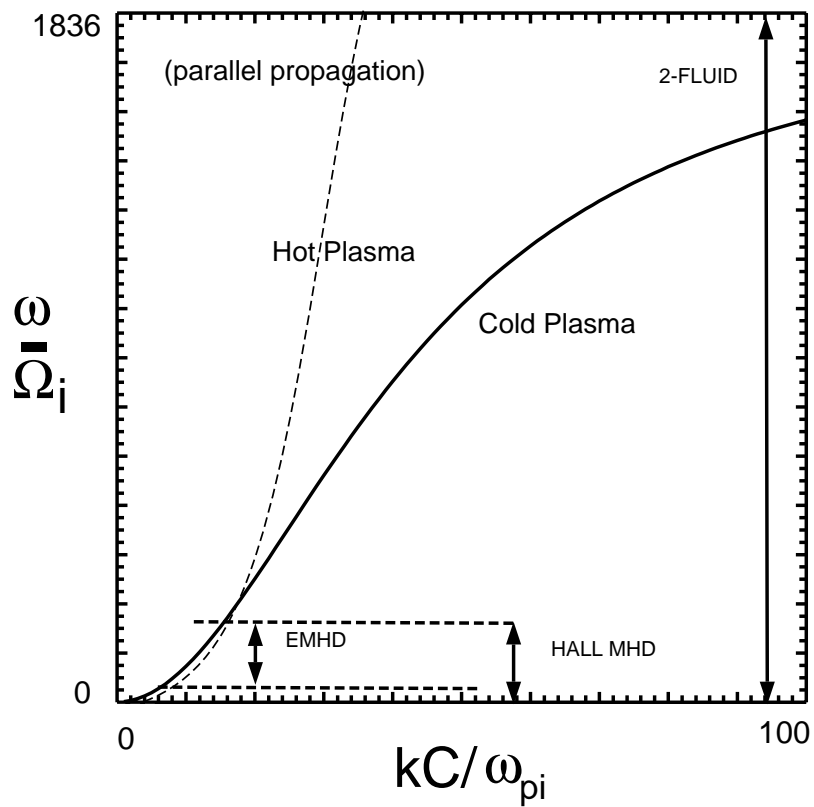
Figure 1.11 Friedrichs diagram for both two-fluid and EMHD dispersion relations (Wang and Kivelson, 1996). The group velocity shows that the energy flow of the whistler wave propagates mainly along the magnetic field. A line has been drawn at an angle of 20° to the $V_{||}$ axis to show that the whistler wave group velocity is constrained to lie in a narrow cone about the background field direction.
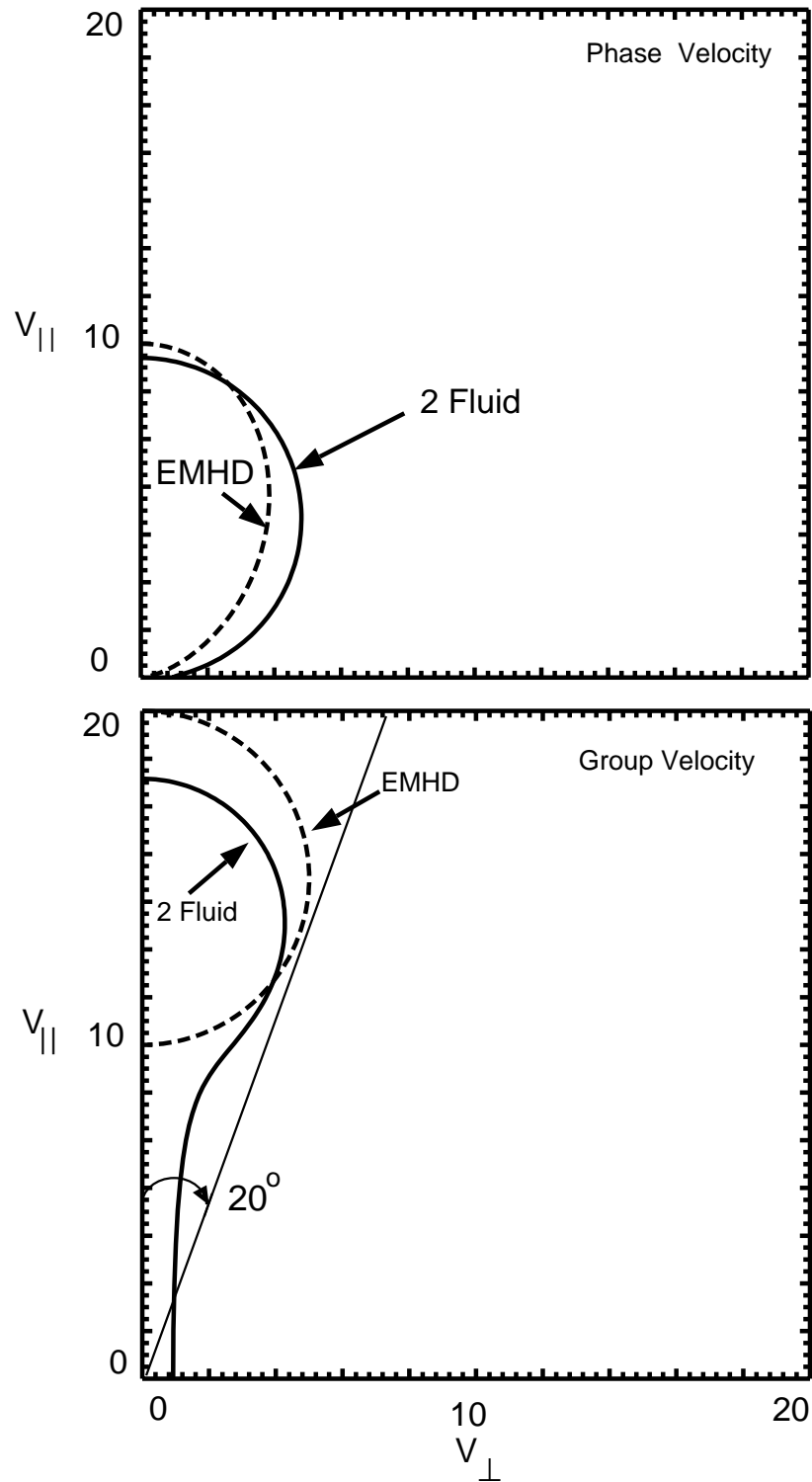
Kivelson et al. (1995) and Wang and Kivelson (1996) have interpreted the magnetic field rotations observed during the Galileo asteroid flybys as evidence that the solar wind is interacting with magnetized asteroids and forming whistler wakes. The magnetic field perturbations associated with a whistler wake are primarily in the transverse components (non-compressional) as observed in the flyby data. Whistler waves are free to propagate upstream in the solar wind which is required to explain the observations at Ida. Solar wind structures unrelated to nearby asteroids but are similar to the observed asteroid signatures are identified in this study. This is accomplished by defining the properties of an asteroid-like signature and then locating these structures in an interplanetary magnetic field dataset. The characteristics of an asteroid-like signature are defined by using a combination of the properties of the observed signatures and the theoretical signatures of a standing whistler wake. After events are identified, their probability distribution function, and hence, the probability of observing an event not associated with an asteroid, is determined. The stability of the result is then tested by varying the parameters that are used in the event selection process.

2 Event Identification and Selection Criteria

In the previous section it was stated that this study seeks to determine the rate of occurrence of small scale (short duration) rotational discontinuities which might be misinterpreted as evidence of an asteroid interaction with the solar wind. The data sets that contain the presumed asteroid signatures were presented and the characteristics of those signatures were discussed. This chapter describes the event selection criteria, and their justification, used to identify similar IMF structures unrelated to the presence of a nearby asteroid.

2.1 Ulysses Data Set

In order to be able to identify IMF discontinuities of short duration, a data set must have adequate temporal resolution to resolve the structures of interest. The available Pioneer 10 and 11, and the Voyager 1 and 2 magnetometer data sets in the solar wind containing the asteroid belt crossings have been resampled to one minute averages (NSSDC Master Directory Listing of Data Sets). These data sets are not sampled frequently enough to identify structures of three minute duration like the Gaspra event. One month of Ulysses magnetometer data, resampled to twelve seconds, were made available to us courtesy of A. Balogh, for the asteroid belt crossing in 1991. Much of the analysis, and the published data plots showing the possible interaction at Ida used ten second averages of the magnetic field (Kivelson et al., 1995). The resampled Ulysses data set has adequate sampling resolution to resolve similar structures of interest. In addition, the Ulysses data set was acquired during the same solar cycle and fairly near in time to the Gaspra data set. The Ulysses asteroid belt crossing magnetometer data set covers one solar rotation in February 1991; the Gaspra encounter was in October 1991, eight months later. Figure 2.1 shows the Ulysses magnetometer data set (about one solar rotation) resampled to twenty minute averages. The plot shows a clearly defined sector structure and field compressions near the sector boundaries; the same features that were identified in the solar wind near the Gaspra encounter (Figure 1.3) . The field magnitude in the lows ($\sim$2 nT) and highs (5–7 nT) are similar to the magnitude during the few solar rotations near the time of the Gaspra and Ida flybys (see Figures 1.3, 1.6).

It is important to search for asteroid-like signatures in data sets acquired at asteroid belt distances from the Sun because the solar wind evolves as is travels through the solar system. The wave dispersion relations which determine the nature of various interactions are functions of the field B and plasma parameters ρ_{sw} vary with heliocentric distance (Hundhausen, 1995). In particular, the interplanetary magnetic field (IMF) strength decreases and its orientation becomes more azimuthal (Parker, 1963) while the solar wind accelerates slightly (Parker, 1958) with heliocentric distance. The net effect of these processes tends to increase the proton and electron gyro radii and decrease their gyrofrequencies with increasing heliocentric distance (Tsurutani and Smith, 1979). Since plasma wavelength minima depend on the particle Larmor radii (Alfvén waves on ρ_{ci} and whistler waves on ρ_{ce}), the thickness of structures generated by these waves will increase with increasing heliocentric distance.

Figure 2.1 Ulysses magnetometer data from the inner asteroid belt (Feb. 1991) in RTN coordinates are shown resampled to 20 minute averages. The data show a more complicated sector structure than was observed later in the year by Galileo. The "toward" sectors are again shaded and the "away" sectors are unshaded. Field compressions, similar to those observed the Galileo asteroid encounters, are observed spanning the sector boundaries on February 3 and February 23.
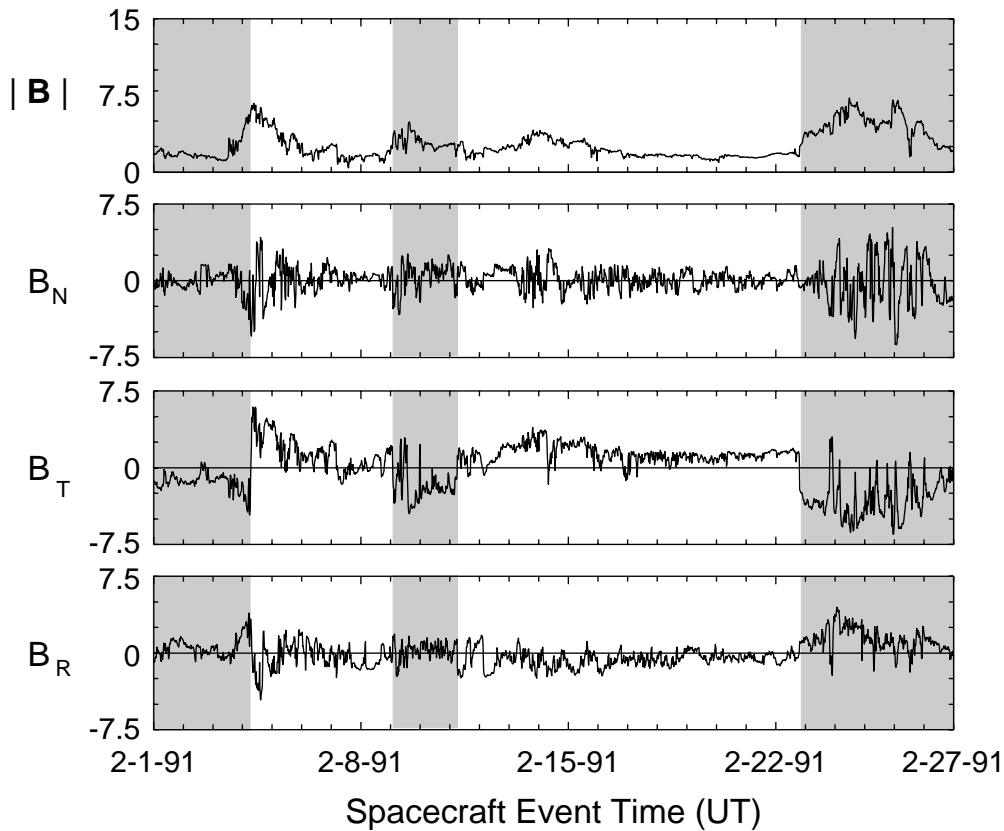
2.2 Interplanetary Discontinuity Detection Methods

Many researchers have studied the rate of occurrence of interplanetary discontinuities (ROID) in the solar wind. The goal of much of this work has been to classify directional discontinuities (DDs) into the subcategories of rotational (RDs) and tangential discontinuities (TDs) in order to study the relative abundances, spatial distribution, sources and evolution of each of these types of solar wind structures. However, there are as many different ways of identifying discontinuities as there are researchers in the field. The two algorithms frequently used to identify and classify DDs today have been put forth by Lepping and Behannon (1986) and Tsurutani and Smith (1979).

Lepping and Behannon (1986) identified, classified, and discussed the characteristics of directional discontinuities observed during Mariner 10's cruise through the inner part of the solar system. For this study they used magnetometer data which had been resampled to 42 second averages. Lepping and Behannon (LB) initially identify DDs using an computer algorithm developed by Sari (1972). The Sari DD detection criteria are as follows: (1) After eliminating obvious noise spikes, the angular change between successive 42 second averages is computed

using $\alpha_t = \cos^{-1}\left(\frac{\mathbf{B_t} \bullet \mathbf{B_{t-3}}}{|\mathbf{B_t}||\mathbf{B_{t-3}}|}\right)$ (2) Those points which have $\alpha_t \geq 30°$ but have missing data within two points before or two points after the change are rejected (i.e., only DDs occurring in relatively continuous data are kept). (3) DDs for which the vector change between either two points before or two points after is greater than $45°$ are also rejected; this disallows interpreting smooth changes as discontinuities. (4) The change in the field calculated from the average of the two points before and the two points after the DD must also satisfy the $\alpha_t \geq 30°$ criterion. (5) Two successive DDs satisfying the above criteria are permitted, but any other DD occurring within four points causes the rejection of both, eliminating step-step or box-like structures (Sari, 1972).

Tsurutani and Smith (1979) studied discontinuities in the solar wind IMF in the region between 1.0 and 8.5 AU using one minute averages of the magnetometer data from Pioneers 10 and 11. In order to carry out this work, Tsurutani and Smith developed a set of DD identification and classification criteria that are less stringent than those put forth by Lepping and Behannon (Tsurutani et al., 1994). Rotational discontinuities are thought to form by phase steepening of Alfvén waves (Cohen and Kulsrud, 1974). Tsurutani et al. (1994, 1996) have provided compelling evidence that Alfvén waves can steepen to form rotational discontinuities and that the ROID increases when Alfvén waves are present. Tsurutani and Smith (1979) argued that since the proton gyro radius increases with distance from the Sun, that it was reasonable to expect that DD's would "thicken" with increasing heliocentric distance. The minimum wavelength of Alfvén waves depends on the proton gyro radius and this in turn affects the thickness of RDs formed by phase steepening. Thick RDs would take longer for a spacecraft to cross and the crossings might not be rapid enough to be identified by the LB selection criteria. In order to allow for thick discontinuities, the Tsurutani and Smith (TS) DD detection method examines the vector change between field vectors separated by three minutes $\Delta \mathbf{B} = \mathbf{B_t} - \mathbf{B_{t-3}}$. The first DD selection criterion is that $|\Delta \mathbf{B}|/\mathbf{B_L} \geq 0.5$ where B_L is the larger of $|\mathbf{B_i}|$ and $|\mathbf{B_{i-3}}|$. Next the variance of the data in the vicinity (but not including) the discontinuity is computed where δ^2 is the larger of

$$\frac{1}{5} \sum_{i=t-3}^{t-7} |\mathbf{B_i} - \mathbf{B_{i-1}}|^2$$

and

$$\frac{1}{5} \sum_{i=t}^{t+4} |\mathbf{B_{i+1}} - \mathbf{B_i}|^2$$

In order to eliminate wave-like structures from being counted as discontinuities, the TS criteria require that $|\Delta \mathbf{B}| > 2\delta$. The final DD selection criterion of TS is that DDs must be separated by at least three minutes. This final criterion ensures that thick discontinuities are not counted more than once.

After directional discontinuities are initially identified, most authors use a variety of methods to classify them as either rotational or tangential discontinuities. In an ideal magnetohydrodynamic (MHD) system, there is no normal component of either the plasma flow ($u_n = 0$) or the

magnetic field ($B_n = 0$) across a tangential discontinuity but these parameters are proportional across a rotational discontinuity $u_n = B_n/(\mu_o \rho)^{1/2}$ (Burgess, 1995). Most of the solar wind studies that have examined the rates of occurrence of directional discontinuities have used data from spacecraft where the plasma data resolution was inadequate to determine u_n across the discontinuity. In order to distinguish between rotational and tangential discontinuities, various methods which relate the size of B_n to the field strength and the change in field magnitude ($\Delta|\mathbf{B}|$) across the discontinuity have been put forth. It can be shown that across an ideal rotational discontinuity in an isotropic plasma, the change in field magnitude should be zero $\Delta|\mathbf{B}| = 0$ while there is no restriction on the change in field magnitude across tangential discontinuities (Hudson, 1970). Table 1, reproduced from Lepping and Behannon (1986), summarizes many of the techniques, including LB and TS, that have been used in these analysis.

All of the DD classification criteria put forth in table 1 make use of the size of ratio of the magnetic field component normal to the discontinuity (B_n) to some representation of the field magnitude (B_L, B_o, etc.). To determine B_n, all of these methods make use of the minimum variance technique described by Sonnerup and Cahill (1967). Minimum variance analysis identifies a discontinuity plane normal ($\hat{n}$) along which the difference vectors ($\Delta\mathbf{B_i}$) have a minimum variation (Lepping and Behannon, 1986). The normal direction is reasonably well determined by minimum variance analysis when the ratio of the intermediate (λ_2) to the minimum (λ_3) eigenvalues of the variance ellipsoid is greater than two, i.e. $\lambda_2/\lambda_3 > 2.0$ (Lepping and Behannon, 1980). The minimum variance analysis used to determine the normal of the discontinuity plane invariably uses the highest data sampling resolution available, even though the discontinuities themselves are identified in data sets with lower sampling resolution. The result of any minimum variance analysis is highly sensitive to the input data. Changes in the data input to the analysis (sampling rate, number of points, field magnitude changes during input interval, etc.) can affect the result or the stability of the result (Lepping and Behannon, 1980). Identification of RDs in the procedures that will be described later are performed in an automated fashion, using 12 second averages of the magnetic field. Discontinuity normals computed in an automated fashion from low resolution data may be less reliable than those performed interactively using high resolution data and carefully selected input intervals.

2.3 Asteroid-Like Event Selection

Wang and Kivelson (1996) have reported on electron magnetohydrodynamic simulations of the interaction between the solar wind and a magnetized asteroid. In this work, the authors set their simulation parameters (relative scale sizes, field strength and direction, flow speed, etc.) to be similar to the conditions present during the Galileo Gaspra and Ida asteroid flybys. Their results show that the interaction is characterized by a series of standing whistler wave fronts. Simulations were run in one, two, and three dimensions. The whistler wave fronts produce a fan shaped disturbance region in the 3–D simulations. The whistler waves are closely confined to the plane defined by the IMF and the plasma flow vectors and are further restricted to be nearly field aligned (within 30°).

Table 2.1 Comparison of various directional discontinuity classification criteria (Lepping and Burlaga, 1986)

Reference	Tangential Discontinuities	Rotational Discontinuities	Mixed (either)	Bad (neither)	Comments
Burlaga et al. [1977] Explorer 43	$B_n < 2$ nT $\sim B_n/B_o < 0.4$	$B_n > 3nT$ $\sim B_n/B_o > 0.6$			B_n/B_o not computed by authors; has been included here for comparision, where we have set $B_o = 5$ nT
Smith [1973] Mariner 5	$B_n/B_L < 0.2$ $\Delta\lvert B\rvert/B_L > 0.22$	$B_n/B_L > 0.4$ $\Delta\lvert B\rvert/B_L < 0.22$			B_L = largest $\lvert B\rvert$ on either side of DD
Tsurutani and Smith [1979] Pioneer 10 & 11	$B_n/B_L < 0.2$ $\Delta\lvert B\rvert/B_L > 0.2$	$B_n/B_L > 0.2$ $\Delta\lvert B\rvert/B_L < 0.2$	$B_n/B_L > 0.2$ $\Delta\lvert B\rvert/B_L < 0.2$	$B_n/B_L > 0.2$ $\Delta\lvert B\rvert/B_L > 0.2$	statisitics computed at 1,5, and 8 AU for "quiet", "active", and "all"
Barnstorf [1980] Helios 1 & 2	$B_n/B_o < 0.3$	$B_n/B_o > 0.5$			B_o = avg $\lvert\mathbf{B}\rvert$ in DD; also used angles relating $\Delta\mathbf{V}$ and $\Delta(\mathbf{B}/\rho)$
Lepping & Behhanon [1980 a, b] Mariner 10	$B_n/B \leq 0.3$ $\sigma_B/B > C$	$B_n/B > 0.3$ $\sigma_B/B \leq C$	$B_n/B \leq 0.3$ $\sigma_B/B \leq C$	$B_n/B > 0.3$ $\sigma_B/B > C$	B = avg $\lvert\mathbf{B}\rvert$ in DD, C = 0.09 at 1 AU C = 0.055 at 0.72 AU C=0.07 at 0.46 AU
Neugebauer et al [1984] ISEE 3	$B_n/\lvert B\rvert \leq 0.4$ $\Delta\lvert B\rvert/\lvert B\rvert \geq 0.2$	$B_n/\lvert B\rvert > 0.4$ $\Delta\lvert B\rvert\lvert\lvert B\rvert < 0.2$	$B_n/\lvert B\rvert \leq 0.4$ $\Delta\lvert B\rvert/\lvert B\rvert < 0.2$	$B_n/\lvert B\rvert > 0.4$ $\Delta\lvert B\rvert/\lvert B\rvert \geq 0.2$	$\lvert B\rvert$ = largest $\lvert\mathbf{B}\rvert$ on either side of DD; also considered differences in plasma properties

Wang and Kivelson examined the 3–D simulations along paths similar to the ones Galileo flew past Gaspra and Ida to see if they resembled the observed magnetometer time series data. Figure 2.2a shows the magnetic field from the Gaspra simulation along a path in the flow-field plane ($V_{sw} = V_{sw}\hat{x}$, $B = B\hat{y}$) similar to the Galileo trajectory (see Figure 1.1). The

Figure 2.2 Magnetic field along two paths through the simulation of the interaction between a magnetized asteroid and the solar wind (from Wang and Kivelson, 1996). A) This slice from (0, 0, Z/2) to (X, Y/2, Z/2), is purely in the X-Y plane where X is taken as the solar wind flow direction and the IMF lies in the Y direction. The perturbation is predominantly in the transverse (X and Z) components of the field. B) This slice is taken between (0, 0, Z) and (X, Y/2, Z/2) and approximates the path of Galileo past the asteroid Gaspra. Note that the perturbation is still predominantly in the Z and X components of the field but that the amplitude of the perturbation is reduced by being out of the plane of the wake wave.

Simulated gaspra figure using Ida plot
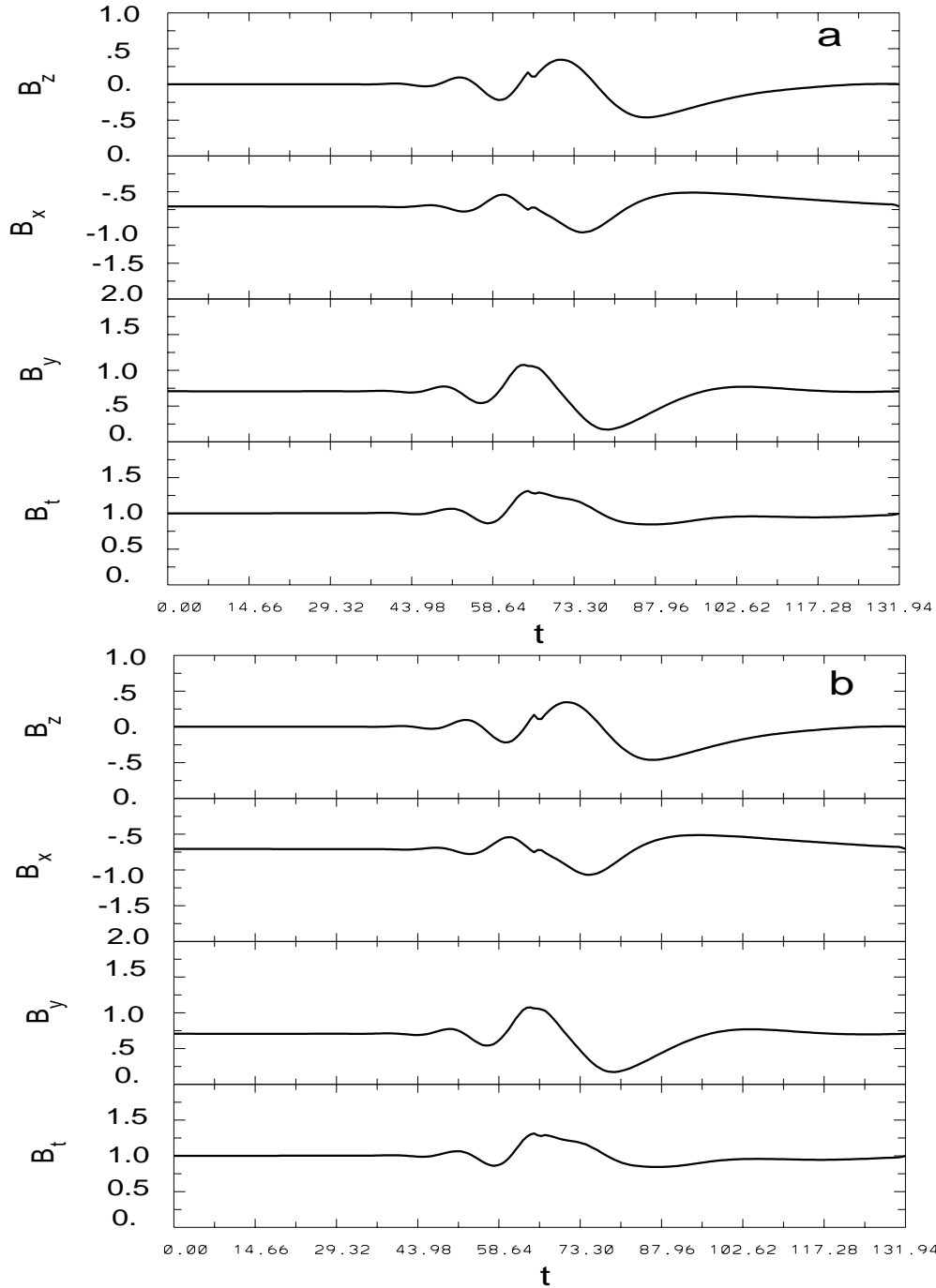
Figure 2.3 (from Wang and Kivelson, 1996) The magnetic field along a path through the Ida simulation box that approximates the trajectory of Galileo past the asteroid Ida $(0, \frac{3}{4} Y, \frac{3}{4} Z)$ to $(X, \frac{1}{2} Y, \frac{3}{4} Z)$. This slice intersects more than a single wavefront and has both "up" and "down" phases of the wave. Again, a finite field compression is observed in the simulation results.
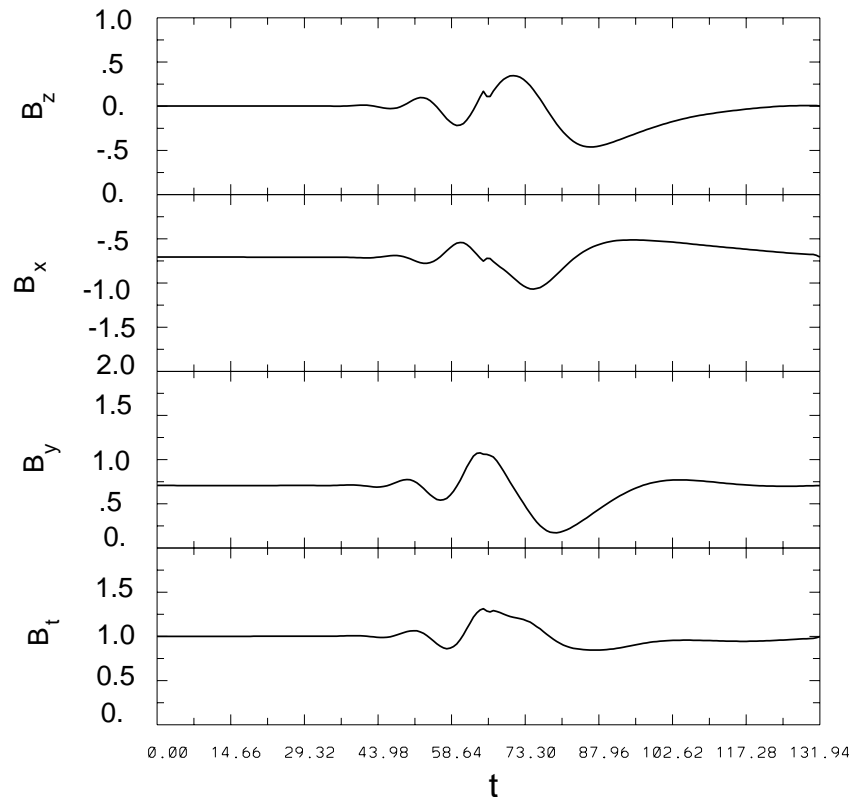
field rotation occurs primarily in the transverse components B_z and B_x and there is a small field compression. The rotations do not appear to be sharp enough to qualify as a rotational discontinuities. The authors argue that the artificial resistivity necessary for numerical stability in the simulation rapidly damps the highest frequencies and smooths the signature (Wang and Kivelson, 1996). If this signature contained the full interaction spectrum, it might more closely resemble the "boxcar" signature observed near Gaspra. Figure 2.2b plots the field from the same simulation as 2.2a along a trajectory that is not purely in the flow-field plane. The field perturbation and compression are strongly reduced out of the plane where the interaction is occurring (Wang and Kivelson, 1996). Figure 2.3 shows the simulated field from the Ida simulation along a path similar to the Galileo Ida flyby trajectory (see Figure 1.2). Recall that the Ida flyby was not in the flow-field plane and that the IMF was not orthogonal to the plasma flow direction during the time of the Ida flyby. The resulting perturbation is observed upstream in the plasma flow, is reduced in amplitude, and has more oscillations than the Gaspra case (Wang and Kivelson, 1996). For this case as well, sharp rotations may be smoothed by the resistivity of the simulation.

Three dimensional simulations provide the opportunity to search for the set of possible theoretical signatures along random trajectories past the asteroid for various IMF orientations

and plasma conditions. In particular, the effects of crossing the flow-field plane at various angles and at various distances from the source on the observed perturbation could be examined. The effort required to characterize those aspects of this problem fully is not warranted here. Wang and Kivelson (1996) have shown that the perturbation decreases in amplitude rapidly with both increasing distance from the source and from the flow-field plane. Qualitatively, the maximum angular perturbations should be observed for wake crossings normal to the wake front and in the flow-field plane (full 180° circular rotations) and the largest amplitude perturbations will be nearest the source. Crossing the wake front at angles away from the wake front normal but still in the flow-field plane should "smear" the signature reducing its sharpness or apparent frequency content. Trajectories that cross the flow-field plane and the wake front will see field perturbations that sweep rapidly, but have less angular change ($< 180^o$) than those crossing within the plane.

Circularly polarized, 180° rotations predicted by the Wang and Kivelson simulations under ideal trajectory and field conditions would be readily identifiable in any magnetic field data set. Realistic combinations of field orientation and trajectory through the simulation box produce a wide variety of potential field perturbations. The observed magnetic signature at Gaspra is characterized by a pair of sharp field rotations (rotational discontinuities) which separate the undisturbed IMF from an asteroid interaction region. This signature is consistent with a trajectory through this simulation near the source in the plasma rest frame and at a low angle to the flow-field plane. At Ida, a more complex and less clearly defined structure is observed. The amount of field rotation at Ida is too small to meet any of the RD identification criteria put forth in Table 2.1, however, the signature is consistent with a trajectory at large distance to the source and parallel to but below the flow-field plane. The key elements of these signatures that suggests an asteroid interaction source are: 1) that the field rapidly rotated when the spacecraft approached the IMF field line connecting the spacecraft to the asteroid, 2) after a few minutes, the field rotated back to an orientation consistent with the trends in the upstream data, and, 3) the field magnitude remained nearly constant over the entire disturbance period (Kivelson et al., 1995). The rapid field rotations, at least for the Gaspra flyby, meet the defining criteria of a rotational discontinuity.

IMF structures, similar to the putative asteroid signatures, are identified for the purpose of determining their occurrence rate. In order to establish asteroid-like event selection criteria, the Ulysses magnetometer data set was visually inspected for features similar in appearance to the Gaspra and Ida perturbations. Sixty-two events were identified. These features all had the following properties: 1) at least one clearly defined rotational discontinuity was present within each signature, 2) the field returned to an unperturbed state after a brief time, and 3) the field magnitude remained nearly constant across the disturbance boundaries and throughout their duration. It is difficult to specify how quickly or slowly the field should return to its background-trending orientation. The size of the asteroid, its presumed magnetic moment, the distance to the asteroid at closest approach, the angle between the spacecraft trajectory and the IMF direction, and the relative velocity between the spacecraft and the wave front can all affect the magnitude and/or duration of the asteroid interaction with the solar wind. In order

to reduce the problem to a manageable number of free parameters, only signatures from small asteroids (1–20 km average radius) are accepted. With this limitation imposed, the duration of possible asteroid-like signatures should cover a range whose minimum (maximum) duration are less (greater) than the observed durations (Gaspra 3.3 minutes, Ida 8 minutes). The duration of an asteroid-like signature is defined to be between 3 and 15 minutes for this study.

The rapid damping of the whistler waves with distance from the source in the Wang and Kivelson (1996) simulation results suggest that a shorter maximum duration might have been appropriate. In nature, electron cyclotron resonance can damp the whistler wave power away from the source (Wang and Kivelson, 1996). However, damping in the simulation is mostly the result of artificial resistivity that is required for numerical stability (Wang and Kivelson, 1996). The maximum event duration was left at 15 minutes to include a maximum number of qualifying events. Justification for the three minute lower limit on the event duration is more problematic. Three minutes was selected in order to eliminate high frequency variations of the IMF direction. The Galileo magnetometer high resolution data near the asteroid encounters show that small fluctuations of 1–2 minutes duration are not uncommon (see Figures 1.4 and 1.7).

In order to make this result consistent with other efforts to identify and classify solar wind discontinuities, existing methods of DD identification and classification as rotational discontinuities were employed. The TS DD identification criteria consistently selects a greater number of events than the LB method (Tsurutani and Smith, 1979) primarily because their criteria allow for thick discontinuities. The TS rotational discontinuity identification were developed for use with magnetometer data sampled once every minute. However, this study seeks to identify short duration structures that were not of interest to Tsurutani and Smith. When applied to a data set sampled every 12 seconds, the Tsurutani and Smith technique of examining the difference between samples separated by three sampling intervals still excludes thick discontinuities, however, the definition of thick changes. Asteroid-like signatures are required to rotate the field more rapidly than other background rotations. The TS criterion that restricts the data variance in the vicinity of the DD in order to eliminate wave-like structures with periods of a few minutes now eliminates waves with periods less than a minute. Although high resolution data are typically used for a minimum variance analysis, high resolution data were not used for this study. The direction normal to the discontinuity is determined here by using a minimum variance analysis over 11 samples (2 minutes) of data centered at each DD. The entire RD identification process was fully automated by using a simple computer algorithm.

After RDs were identified in the data set by using computer algorithms based on the selection criteria summarized in Figure 2.4, the individual RDs were each visually examined to see if the IMF rotated back to its background trend after a few minutes. Considerable effort was made to develop an automated procedure to perform this function so that the results would be reproducible by others. Unfortunately, none of the numerous attempts to develop quantitative criteria to determine when the field returned to an unperturbed orientation was successful. The problem was that detrending data containing a step-function discontinuity changes the step-function character

Figure 2.4 Rotational discontinuity identification criteria as defined by Tsurutani and Smith (1979). Criteria 1–3 identify directional discontinuities in the IMF. Rotational discontinuities are the subset of discontinuities which in addition meet criteria 4–6 after the discontinuity has been analyzed by the minimum variance technique of Sonnerup and Cahill (1967). These equations have been applied to the 12 second sampled magnetometer data from the Ulysses magnetometer in order to identify rotational discontinuities which may also have asteroid-like signatures. The minimum variance analysis used 2 minutes (11 samples) of data centered on the DD.

1) $\dfrac{|\Delta \mathbf{B}|}{B_L} > 0.5$ Where $\Delta \mathbf{B} = \mathbf{B}_i - \mathbf{B}_{i-3}$ and B_L is the larger of B_i and B_{i-3}

2) $|\Delta \mathbf{B}| > 2\delta$ where δ^2 is the larger of

$$\frac{1}{5} \sum_{j=i}^{j=i+4} \left| \mathbf{B}_{j+1} - \mathbf{B}_j \right|^2 \quad \text{and} \quad \frac{1}{5} \sum_{j=i-3}^{j=i-7} \left| \mathbf{B}_j - \mathbf{B}_{j-1} \right|^2$$

3) Discontinuities must be separated by at least 3 samples

4) $\dfrac{\lambda_2}{\lambda_3} > 2.0$ where λ_2 and λ_3 are the intermediate and minimum eigenvalues from the minimum variance analysis

5) $\dfrac{B_n}{B_L} > 0.2$ where B_n is the component of $\mathbf{B}$ normal to the discontinuity plane

6) $\dfrac{\Delta |\mathbf{B}|}{B_L} < 0.2$ across the discontinuity plane

of the discontinuity. After detrending, step-function structures become structures with a sharp onset and a gradual return to the background orientation. Identifying and separating short duration rotations from step-function discontinuities from the selection set is one of the primary goals of this procedure.

Short duration fluctuations from a background orientation are only of interest here if they are an anomalous rather than a pervasive state of the IMF (not wave trains) . As such, events can only be identified in regions of high data continuity where the baseline conditions can be established. This imposes the need for an event selection criterion requiring that events occur in regions of high data continuity. If more than ten percent (10%) of the data in the one hour

Figure 2.5 Cartoon illustrating the possible forms of an asteroid signature in the magnetic field component with the maximum variance. Four types of possible signatures are shown: 1) shows an idealization of the box-like structure, 2) shows the square-wave structure, 3) shows a sharp rotation followed by a gradual return to background conditions, and 4) is the inverse of 3).
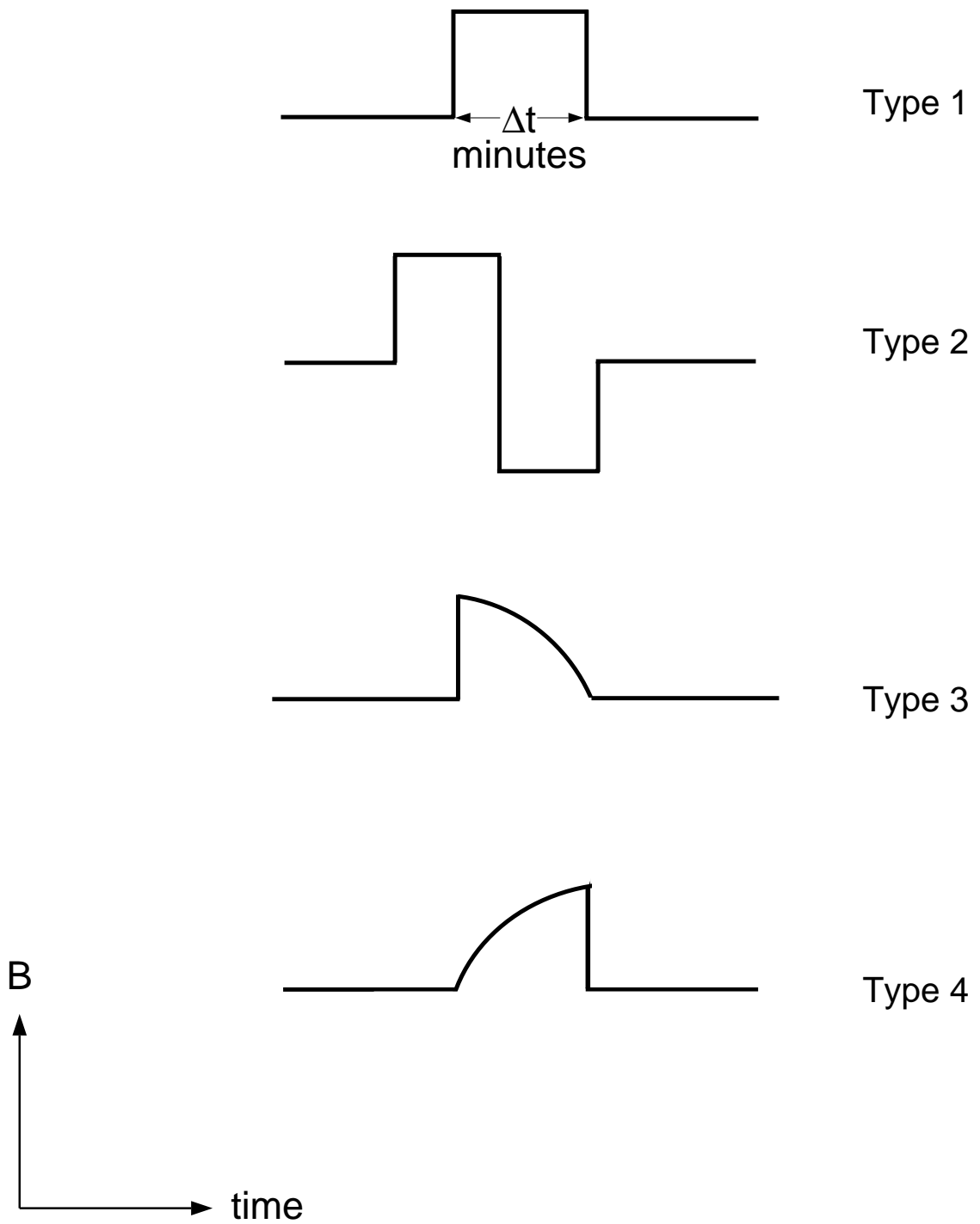
Figure 2.6 Examples of the four types of asteroid-like signatures, plus an example of a rotational discontinuity that does not meet the asteroid selection criteria, from the Ulysses data set. Asteroid-like signatures are the shaded portion of each vertical panel. Each vertical panel in the figure contains thirty minutes of data; however, the data in the panels are not contiguous. Data are shown on a 5 nT scale, the horizontal line in the component panels is zero. Panel 1 provides an example of a box-car type signature of about eight minutes duration. Panel 2 shows a square-wave signature of about twelve minutes duration. Panels 3 and 4 show examples of structures with only one rotational discontinuity, with either a sharp onset (3) or sharp return (4). The last panel (5) shows a "step-function" rotational discontinuity which is not considered to be asteroid-like because the field does not return to its unperturbed orientation.
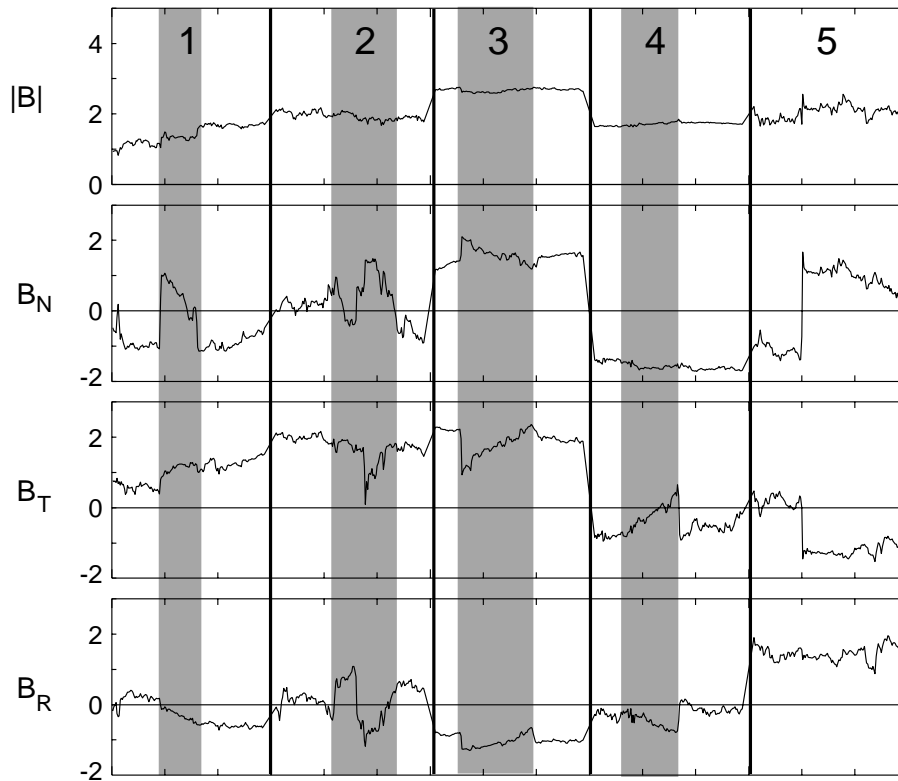
interval centered on a potential event is lost, then the event is not selected. A second data continuity requirement eliminates potential signatures where any part of the signature is lost to a data gap. These requirements were imposed during the visual selection process. Tools in the IGPP data display software (King et al., 1988) provide accurate determination of the duration of data gaps from data plots on a computer screen.

The field magnitude is not expected to change as a result of a whistler mode rotation of the magnetic field. However, the Wang and Kivelson (1996) simulations do show finite perturbations in the field magnitude. A small amount of compression is allowed in the whistler mode solution for waves not propagating purely parallel to the field. The final asteroid-like signature selection criteria is that the field magnitude may not vary by more than twenty percent over the event

duration. The previous magnitude change requirement was only applied across the rotational discontinuity.

Figure 2.5 is a cartoon which shows four idealized cases of signatures in magnetometer data that this study would identify as being asteroid-like. Type 1 events have a box-car signature similar to the Gaspra observation. Type 2 events have the square-wave appearance of the Ida signature. Type 3 events have a sharp rotational discontinuity with a gradual return to the background orientation and type 4 events are the reverse of type 3. Event types 3 and 4 were not observed near asteroids but have been included as possible signatures of asteroids, possibly from an oblique crossing of a whistler wake.

Figure 2.6 shows examples selected from the Ulysses data set of each of the four types of idealized asteroid-like signatures, plus one example of a rotational discontinuity that does not meet the asteroid selection criteria. The data are organized into vertical panels where each panel contains 30 minutes of data. The time intervals selected for the figure are not contiguous. Shading is used to identify the signatures within each panel. Panel 1 contains a type 1 event, panel 2 contains a type 2 event, etc. The last panel (5) shows a "step-function" rotational discontinuity which is not considered to be asteroid-like because the field never returns to its unperturbed orientation.

To summarize, asteroid-like events, in addition to meeting all of the requirements of a rotational discontinuity, satisfy:

1. the duration of the event is between three and fifteen minutes,
2. the field magnitude does not change by more than 20% over the duration of the event,
3. the data are continuous (no flagged data or missing records) for the entire event duration, plus three records on each side of the event, and
4. the hour centered on the event has at least 90% data continuity.

The Gaspra signature meets all of these requirements. The Ida signature does not meet the requirements because it does not contain a rotational discontinuity; the angular rotations simply aren't large enough because of the background field strength. Signatures similar in structure to one observed near Ida (square-wave) are included in these selection criteria because simulation results indicate that a square-wave is a possible signature.

3 Statistical Results and Analysis

This chapter reports the results of the search for asteroid-like signatures in the IMF at a heliocentric distance of 2–3 AU from the Sun in the ecliptic plane. The search technique described in the previous chapter was applied to twelve second averages of the IMF acquired by the Ulysses magnetometer (Balogh et al., 1992) as the spacecraft traversed the asteroid belt. The data were acquired directly from the principal investigator, Dr. Andre Balogh.

Before proceeding with the search for asteroid-like signatures in this data set, it was necessary to determine whether or not the IMF during this period was in any way anomalous. This study of the rate of occurrence of special IMF microstructures (asteroid-like signatures) is relevant only if the overall structure was characteristic of the IMF at these radial distances. No previous studies have focused on the solar wind or IMF microstructure specifically at this heliocentric distance. However, Tsurutani and Smith (1979) studied the IMF microstructure as a function of radial distance from 1–7 AU by using data acquired by Pioneers 10 and 11. They were able to separate temporal variations of the rate of occurrence of interplanetary discontinuities (ROID) from spatial variations (radial gradient) through the use of two spacecraft. The observed radial gradient in the ROID was well represented by the equation $\rho = 41 \exp^{-(R-1)/4}$ or, more precisely, $log_{10}(\rho) = (1.61 \pm 0.04) + (-0.07 \pm 0.01)R$ where ρ is the ROID, R is the radial distance from the Sun in AU, and the standard errors of the regression are given as the uncertainties in the second equation (Tsurutani and Smith, 1979). Applying this equation, one would expect to find about 30 discontinuities per day a solar distances between 2 and 3 AU.

Figure 3.1 shows how Tsurutani and Smith determined the radial gradient in the ROID from their data. The top panel (A) shows the solar rotation averages of the ROID (discontinuities/day) for both spacecraft plotted as a function of solar rotation number (time). Pioneer 11 was launched after Pioneer 10 and remained nearer the Sun than Pioneer 10. Pioneer 11 also saw a greater number of discontinuities over the entire interval plotted. The bottom panel (B) shows the ROID of both spacecraft, projected back to 1 AU using the equation for the radial gradient, plotted versus solar rotation number. After correction, the large scale, low frequency, structure is very well correlated for the two spacecraft. The degree of correlation (0.86) after the radial gradient is removed indicates that the radial gradient is both real and well described (Tsurutani and Smith, 1979).

Another feature of the IMF microstructure that is readily apparent in Figure 3.1 is the large variability in the ROID, even after solar rotation averages have been taken. Shortly after launch, at a distance of 1.1 AU, Pioneer 11 observed 56.2 ± 21.1 discontinuities per day (Tsurutani and Smith, 1979). At the same radial distance, Pioneer 10 observed 37.5 ± 17.8 discontinuities per day (Tsurutani and Smith, 1979). Daily averages of the ROID at 1.1 AU varies by an order of magnitude and solar rotation averages vary by a factor of 2.5 (Tsurutani and Smith, 1979).

Figure 3.1 (Tsurutani and Smith, 1979) Panel A shows solar rotation averages of the number of discontinuities per day for both Pioneer 10 and 11 plotted against the Bartels solar rotation number. At the top of the panel, the heliocentric radial distance is plotted for both spacecraft. There are no data during the jovian encounter periods. Note that Pioneer 11 always observes more discontinuities than Pioneer 10, and that the difference between the two curves seems to track the radial separation between the two spacecraft. Panel B shows the discontinuity rate for both spacecraft projected back to 1 AU assuming a radial gradient of $\rho = 41e^{-(R-1)/4}$, where ρ is the number of discontinuities per day and R is the distance from the Sun in AU. The correlation between the number of events for the two spacecraft is 0.86. The high correlation indicates that the radial gradient is well predicted. The differences between the two curves indicate that there are processes besides a simple radial gradient that are affecting the number of discontinuities observed.
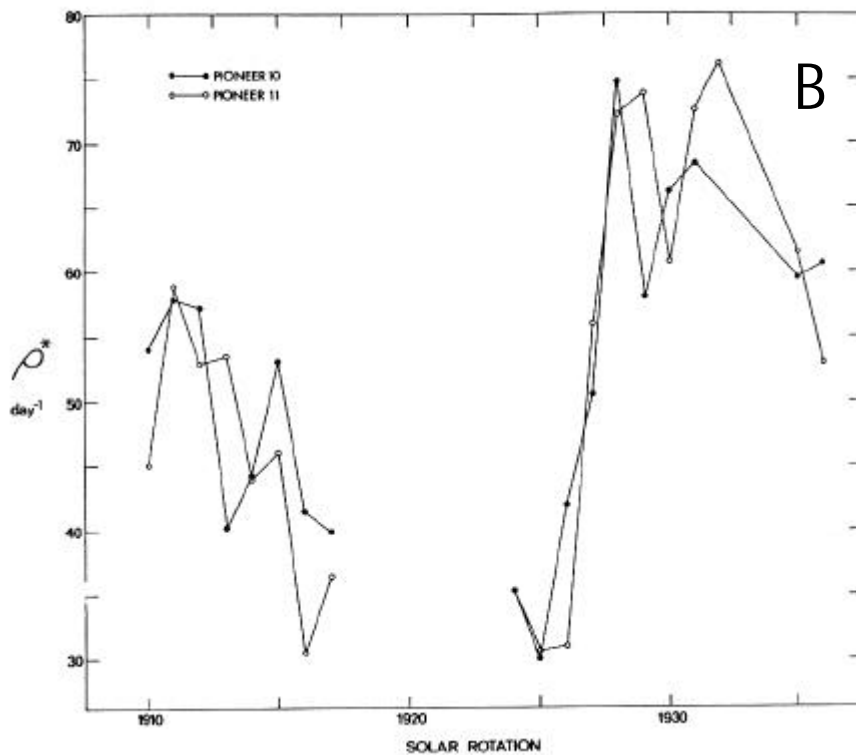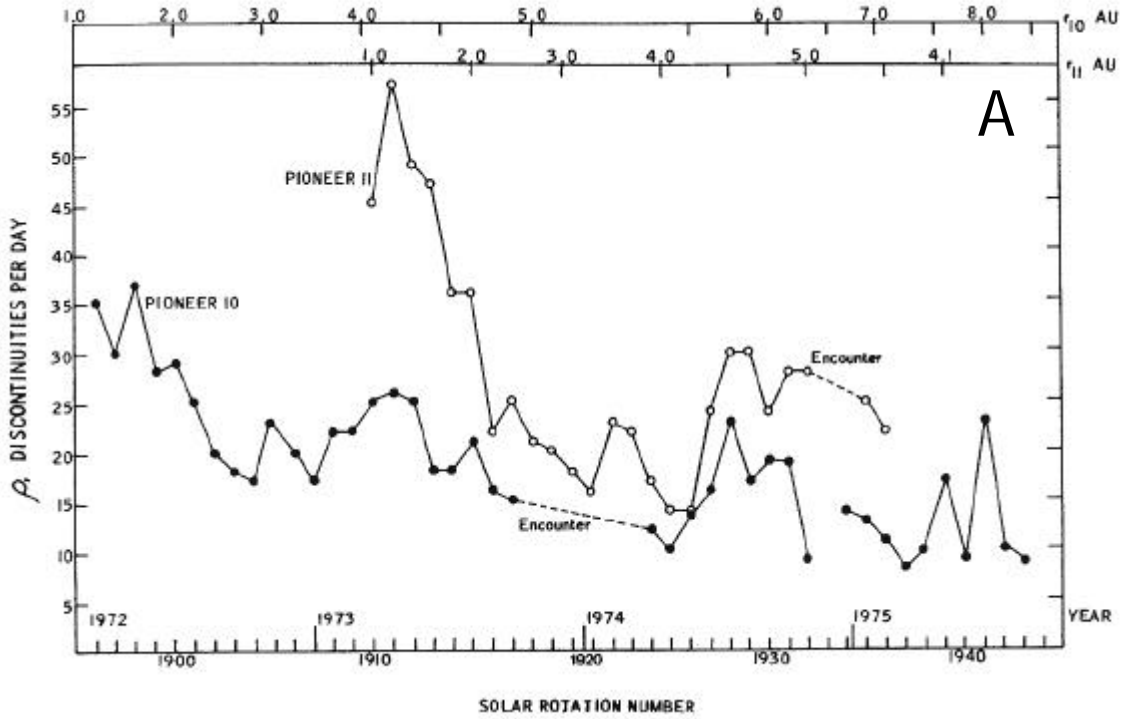
Similar variability in solar rotation averages of the ROID are apparent in Figure 3.1 for Pioneer 10 out to 8 AU.

The Ulysses data set from one solar rotation at 2–3 AU was used to calculate the ROID satisfying the Tsurutani and Smith ROID criteria. The data were first averaged down to one minute samples to apply their selection criteria. Daily averages of the ROID were computed. The average of these values over the solar rotation was determined to be 30.1 $\pm$3.6 where the uncertainty is the standard error of the mean. This number compares very favorably with the range of 25–32 predicted by the Tsurutani and Smith equation for radial distances of 3 and 2 AU respectively. In addition, there is an order of magnitude range in the daily average ROID which is also consistent with the Tsurutani and Smith result. These results suggest that the solar wind conditions sampled by Ulysses in February 1991 were representative of average conditions, in both mean and variance, for that region of interplanetary space.

Figure 3.2 shows 20 minute averages of the Ulysses magnetometer data for the entire solar rotation and shows histograms of the number of rotational discontinuities[6] and asteroid-like events[7]. There are several interesting features evident in this plot. First, the number of discontinuities per day varies greatly, from 2 to 68, while the number of asteroid-like events varies from 1 to 24. High variability in the ROID is a pervasive characteristic of the IMF. Tsurutani and Smith (1979) found four daily averages in a 27 day sample that differed from the mean by more than four standard deviations. Variations from the mean of that size and frequency are well outside of the expected range of statistical fluctuations expected for a Poisson distribution[8] (Tsurutani and Smith, 1979). Tsurutani and Smith have interpreted this variability as an indication that the distribution function is not stationary; that the mean of the distribution varies with time (Tsurutani and Smith, 1979). Another prominent feature evident in this plot is the strong correlation between the total number of rotational discontinuities per day and the number of asteroid-like signatures per day. This is not surprising. Asteroid-like signatures are a subset of the larger population and one would expect that an increase in the parent population would be reflected in the subset. Another important feature is that the number of discontinuities is anti-correlated with the field magnitude and the level of fluctuations in the field components. The relationship between the number of discontinuities and field magnitude is a direct result of the $\frac{|\Delta B|}{B}$ selection criterion. On the other hand, one might expect that the number of rotational discontinuities increases when the field components fluctuate, yet this is not observed. Both types of discontinuities occurred most often on February 19 and 20 when both the field magnitude ($\sim$2 nT) and the total variance of the field components were at their minima. Tsurutani and Smith left many aspects of the variability of the ROID unexplained. In particular, they did not report observing an anti-correlation between the ROID and the field magnitude or large variability in the field components.

---

[6]   The rotational discontinuities in Figure 3.2 were identified using the selection criteria summarized in Figure 2.4

[7]   Asteroid-like events are RDs that additionally satisfy the conditions summarized in the final paragraph of Chapter 2. The details of the identification process are described in the next section.

[8]   A Poisson distribution is a special form of the binomial distribution function that applies when the number of "selected" events is much less than the number of samples. The Poisson distribution is generally appropriate for counting experiments where the data represent the number of observed events per unit time (Bevington, 1969)

Figure 3.2 Panel A plots the number of RDs (solid) and asteroid-like signatures (dashed) observed per day versus the day number of February, 1991. The mean values (μ) are assigned uncertainties equal to the standard errors of the mean. The traces appear to track each other as expected when a random subset of a population is plotted with the parent population. Panel B shows the 27 days of Ulysses magnetometer data averaged to 20 minute samples.

Events per Day

A

All RD's $\quad \mu = 23.6 \pm 3.0 \quad \sigma = 15.4$
Asteroid-like $\quad \mu = 8.6 \pm 1.2 \quad \sigma = 6.1$

Ulysses Magnetometer Data <nT>

B

$|\mathbf{B}|$

B_N

B_T

B_R

2-1-91   2-8-91   2-15-91   2-22-91   2-27-91
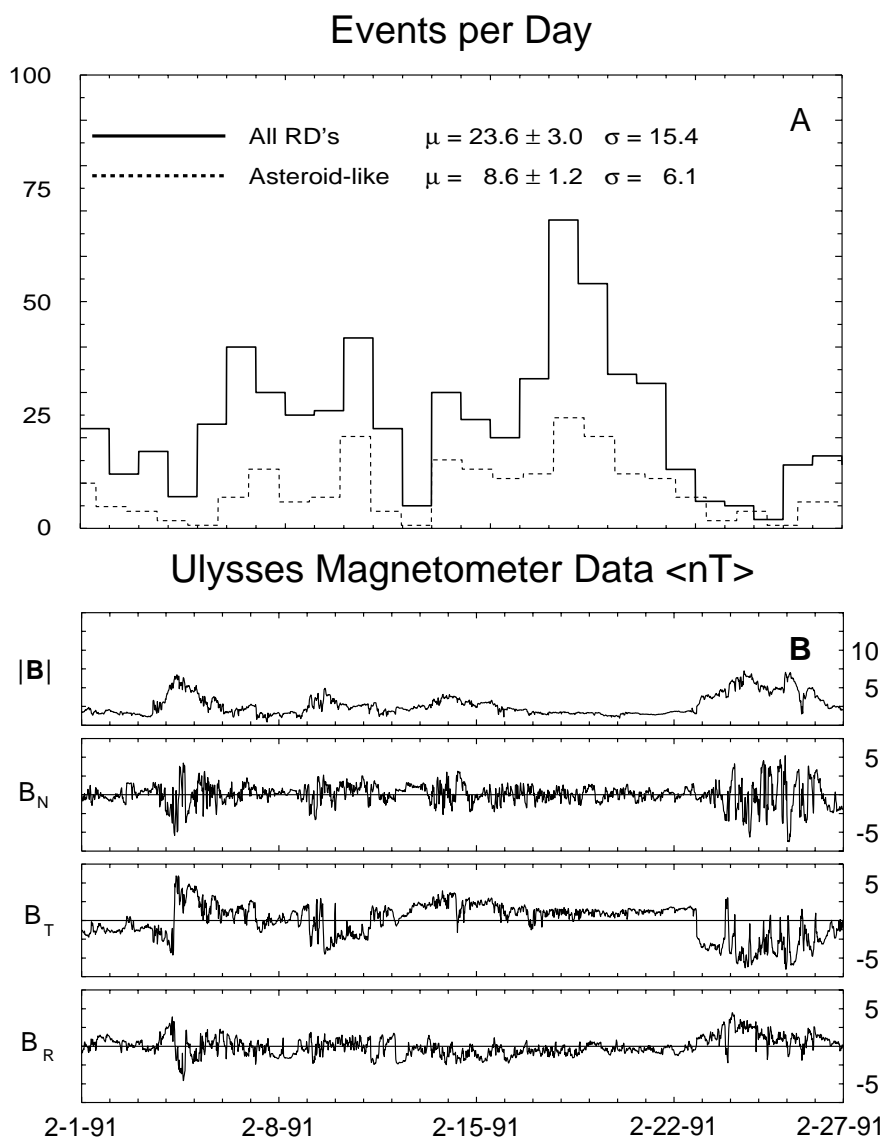
3.1 Results

The previous section describes tests used to establish that the IMF microstructure of the source data set is representative of the nominal solar wind at asteroid-belt distances from the Sun. This section describes the results of the search for asteroid-like signatures in the source data set. Rotational discontinuities were identified by software that applied the selection criteria described in the last chapter (see Figure 2.4). This software, called *discontinuity*, is written as an analysis application that is part of the UCLA/IGPP Data Flow System (King et al., 1988). A detailed description of the software input and output is provided in Appendix C. The automated discontinuity detection software identified an average of 24.7 ± 3.0 rotational discontinuities (RDs) per day in the data set containing twelve second averages. This value is smaller than the number identified in the one minute averaged data set primarily because only rotational discontinuities are counted. The ROID value of 30 counts per day includes all directional discontinuities (DDs), not just rotational discontinuities. In addition, thick discontinuities are counted at low sample rates but are disallowed when the selection criteria are applied to higher time resolution data. In thick discontinuities the field may not rotate fast enough to be selected when the time between samples is short.

This number ($\sim$25/day) is not as low as might be expected. Neugebauer et al. (1984) applied the Tsurutani and Smith DD selection criteria to 1 minute/sample data acquired at 1 AU and found that only about 60% of the DDs identified satisfied the RD requirements. The loss of these discontinuities is compensated to a large degree by additional shorter duration discontinuities in the higher time resolution data set. In a data set sampled every minute, rotations large enough to be counted are discarded if they occur within three minutes (samples) of another rotation. These events are eliminated in order to prevent long, slow, changes in the IMF direction from being considered as discontinuities. This selection criterion also eliminates box-car structures. When the sample rate is increased, short duration events that might have been rejected are counted.

After rotational discontinuities were identified, each one was visually inspected to determine if the other requirements for classification as an asteroid-like signature were met. All events were classified as type 1, 2, 3, or 4 events (box-car, square wave, etc.). The visual inspection was performed twice, at times several months apart, in order to ensure that the visual selection criteria were being applied consistently. The visual selection criterion requiring 90% data continuity in the hour centered on a potential event was added after the first visual inspection. For the most part, the data are quite continuous. This requirement was added because the data continuity is low on two successive days (Feb 5–6). Most of the two days with poor data continuity were eliminated from the data set during the second inspection. The average number of events per day was reduced from 10.08 to 8.96 between the first and second inspections. Figure 3.3 shows the number of events selected from the first inspection by using dashed lines and the second inspection by using solid lines. The 2 days of low data continuity are shaded. There is a systematic reduction in the number of events identified in the second pass of about 1 event per

day. Of the 231 events selected in the second inspection, only 3 events were not selected in the first inspection. The shift between the two applications of the visual selection criteria may be related to the additional data continuity requirement. Alternatively, the selection criterion requiring that the field orientation return to an unperturbed state could have been applied more restrictively during the second inspection. This is the most subjective of the visual inspection criteria and is likely to be the one applied inconsistently between inspection passes.

Event types 3 and 4 (rapid onset, gradual return and vice-versa) were added to the selection set even though these types of signatures were not observed during the Galileo asteroid flybys in order to include additional signatures that might be feasible for a whistler wake crossing. Tsurutani has suggested (personal communication, May 1996) that at least some of these event types appear to be Alfvén waves that have just steepened to form rotational discontinuities. Tsurutani suggested that these event types be eliminated from the selection set. On inspection, some of these events occur in clusters associated with Alfvén wave trains and others do not. In order to ensure that a maximum rate of occurrence of asteroid-like events is computed, event types 3 and 4 were not eliminated from the results.

Figure 3.3 Comparison of counts of events obtained by visual inspections performed several months apart. The number of observed asteroid-like events per day selected during the first inspection (Jan 1996 – dashed line) and the second inspection (June, 1996 – solid line) are plotted. The visual selection criteria were modified to include a data continuity requirement after the first inspection. The region shaded in gray indicates 2 days with very poor data continuity which significantly alters the results of the two inspections. These 2 days of data were eliminated from the data set before statistical parameters were calculated.
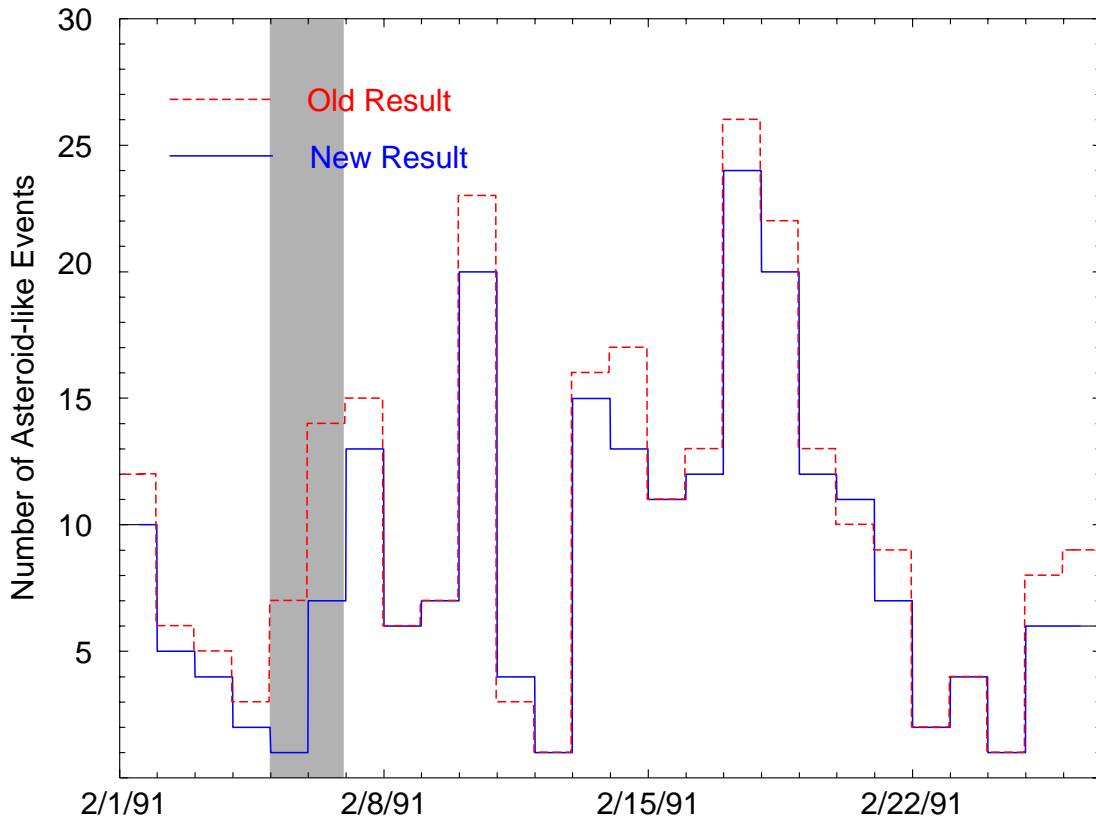
The statistical properties of the observed distribution of asteroid-like events from the second inspection are summarized in the following table: Parameters are given for both daily averages

Table 3.1 Statistical parameters of the observed asteroid-like events.

All Events

Average number	8.96 / day
Standard deviation	6.17 / day
Standard error of the mean	1.23 / day
Median	7 / day
Mode	4 or 6 / day
Average event separation time	161 minutes
Standard deviation (separation time)	233 minutes
Standard error of the mean (separation time)	22 minutes
Median event separation time	79 minutes
Mode of event separation times	20-39 minutes

of events and for the separation times between individual events. Note that the average number of events per day and the average event separation times are consistent but that the median and mode values are not. The median daily rate indicates that there are as many days with fewer than 7 events per day as there are days with more than that number. If the events were uniformly distributed over the interval, one would expect that the median event separation time would be on the order of 200 minutes $\approx \frac{1440 minutes/day}{7 events/day}$. Similarly, the mode of the daily rate would predict about 300 minutes as the most likely event separation time. The fact that the median and mode of the event separation times differ so much from the average daily rate indicates that the events are not randomly distributed over the interval. The distribution of these events must be highly skewed.

3.1.1 Result Sensitivity to Selection Parameters

The criteria used to select asteroid-like signatures are arbitrary. Every effort was made to select parameters that would overestimate the number of events while still selecting events with the appropriate characteristics. Each of the parameters used in the automated rotational discontinuity selection process was individually varied to determine its effect on the selection process. The details of this parameter search are provided in Appendix B. The RD classification criteria of Neugebauer et al. (1984) were used as a starting point. The signature observed near Ida does not meet the Neugebauer RD selection criteria. Since this signature is thought to be related to the asteroid flyby (Kivelson, et al., 1996), an attempt was made to modify the criteria so that the Ida event would be selected. After each modification, the rotational discontinuities identified by the automated process were visually examined. If many of the selected events

would not have been selected by visual inspection, or vice-versa, then the selection criteria were tightened or relaxed as needed. However, changes that selected the Ida signature, accept too many other events that did not pass visual inspection as legitimate rotational discontinuities. Thus, the final criteria were set so that the Ida signature is not selected.

The selection criterion that most significantly affects the number of rotational discontinuities identified is $\frac{|\Delta \mathbf{B}|}{B}$. The requirement that this ratio be greater or equal to 1/2 is equivalent to requiring that the field rotate by at least 30° across a RD. This parameter was varied between values of 0.1 and 1.0. When this ratio fell below 0.4 events that are clearly not rotational discontinuities were selected and thousands of events were selected each day. At Ida, this ratio was about 0.2

A significant factor in the selection of rotational discontinuities, and hence of asteroid-like events, is the field magnitude. The field magnitude is used in the scaling of the event selection parameters to ensure that they remain constant in a relative sense (proportionate effect). However, when the field magnitude increases, many of these criteria simultaneously become more restrictive in an absolute sense. Larger perturbations are needed to satisfy selection criteria that are scaled by the field magnitude. In Chapter 1 it was noted that the size of the perturbations at Gaspra and Ida were nearly equal in amplitude, about 1 nT. The Gaspra perturbation occurred in a 2 nT field while the Ida signature occurred in a 4 nT field so the perturbation produced a smaller field rotation at Ida; too small to satisfy the selection criteria. Figure 3.2 shows that the largest number of events, both rotational and asteroid-like discontinuities, occur when the field magnitude is low and vice-versa. This is consistent with a bias towards selecting events in low fields where small changes can correspond to substantial field rotations.

The statistical result was tested for bias against events occurring during periods of enhanced field magnitude by applying alternative discontinuity identification criteria to the data. The alternative requirements accept perturbations of magnitude greater than 1.0 nT where the standard requirement is that the ratio of the magnitude of the perturbation to the field magnitude is greater than 0.5. Scaling perturbations by the field magnitude filters out events that are not significant with respect to the background field. In this test we require that the perturbation be substantially larger than fluctuations in the vicinity of the event. The requirement is that magnitude of the perturbation is more than 3 times the magnitude of the standard deviation (δ) of the data in the vicinity of the potential event. Thus, both selection criteria 1 and 2 were modified during this test. All other event selection criteria were unchanged. Table 3.2 compares event selection criteria 1 and 2 for the standard identification technique to those used in this test.

Criterion Number	Standard Criteria	Alternative Criteria
1	$\frac{\Delta \mathbf{B}}{\mathbf{B}} > 0.5$	$\Delta \mathbf{B} > 1 \mathbf{nT}$
2	$\frac{\Delta \mathbf{B}}{\delta} > 2.0$	$\frac{\Delta \mathbf{B}}{\delta} > 3.0$

Table 3.2 Test for event selection criteria bias. The standard criteria are those used by Tsurutani and Smith (1979) to identify DDs. The alternative criteria are alternatives to the Tsurutani and Smith criteria that are not biased against events in large fields.

Figure 3.4 Comparison of the number of RD events selected using the nominal selection criteria and a modified set of criteria that should eliminate any bias against events during enhanced IMF strength. The dashed trace is the nominal result based on the Tsurutani and Smith (1979) and Neugebauer et al. (1984) identification criteria. The solid line shows the result for the alternative criteria in Table 3.2. At the bottom of the plot is the Ulysses field magnitude averaged to 20 minute samples. The anti-correlation between the number of observed events and the field magnitude is no longer present in the data represented by the solid line.
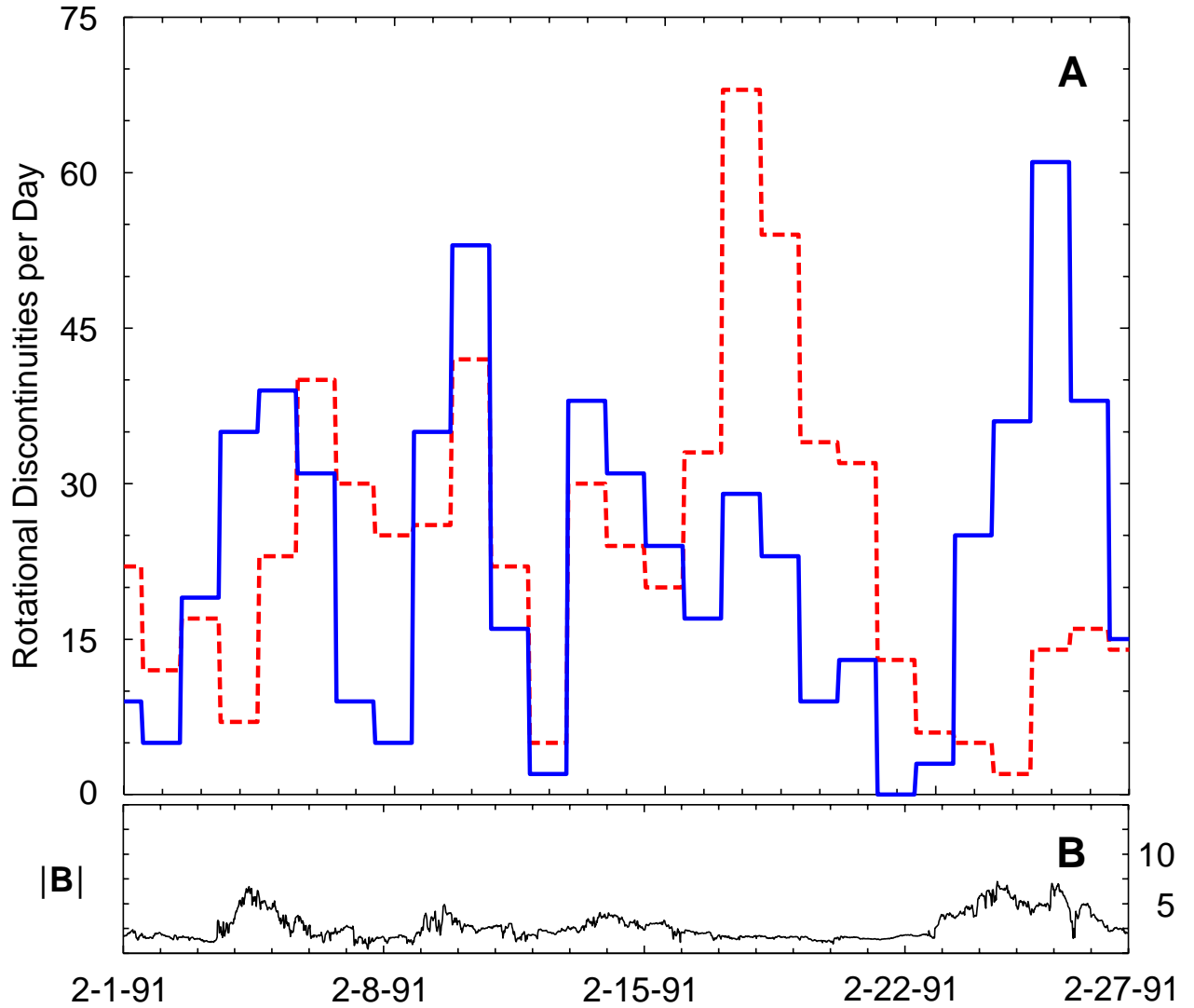
Figure 3.5 shows a histogram of the number of RD events identified each day by using the two selection criteria and the field magnitude as observed by Ulysses. The standard selection criteria events are the dashed line, the alternative criteria results are the solid line. The two traces are both remarkably different and remarkably similar at the same time. The maximum number of events identified by each set of criteria occurs when the number of events identified by the other criteria is about average. The minimum event days are more closely correlated between the two techniques. There does not appear to be any systematic shift, in either time or number of events, between the two traces. The apparent correlation between the field magnitude and the number of events in the standard selection criteria is not apparent in the results of the test criteria. On the other hand, both traces have similar maxima, minima and overall variability. In fact, nearly all of the moments of the two distributions are the same. Table 3.3 summarizes the statistical parameters of the distributions generated by the different event selection criteria.

Table 3.3 Rotational discontinuity distribution moments for nominal and alternative event selection criteria

Parameter	Standard Criteria (events/day)	Alternative Criteria (events/day)
mean	23.6	23.0
error of the mean	2.96	3.05
standard deviation	15.4	15.9
median	22	23
mode	5,14,22,30	9
minimum	2	0
maximum	68	61

The test for bias in the result generates a distribution of events that are identified as rotational events, not as asteroid-like events. Presumably the visual inspection process would eliminate a similar number of events from each of the two distributions producing similar asteroid-like event distributions. However, the apparent bias against events occurring in regions of enhanced field strength would not be present in this distribution. This test result suggests that even if a bias is present in the RD selection criteria, the moments of the distribution are unaffected by this bias.

No records were made to identify which of the visual inspection criteria were violated when events were discarded. As discussed in the previous section, the application of the visual inspection criteria was performed consistently in two separate applications, with the possible exception that the event duration requirements may have been applied more restrictively during the second application. The event duration requirements that the field rotate back to its background trend within 3 and 15 minutes of the rotation onset were clearly the most restrictive of the event selection criteria. Of the 686 rotational discontinuities, only 231 were found to

satisfy all of the visual inspection criteria. Results from visually inspecting the data twice, with and without the two data continuity requirements, demonstrates that these criteria eliminate a maximum of 45 events or 10% of the total number of events discarded. There was a visual inspection criterion that the field magnitude remain constant (within 20%) over the duration of the event. This criterion eliminated less than 20% of the RDs identified by software. Even though the event duration requirements were applied loosely, and far fewer events should probably have passed through this filter, these selection criteria eliminated most of the events disallowed by visual inspection.

The distribution of the selected event durations provides information about the sensitivity of the result to the bounding values selected. The number of selected events of a given duration is plotted versus event duration in Figure 3.4. There appears to be a substantial fall-off in the number of events selected as the duration increases from 5 to 14 minutes followed by a slight rise in the number of events of 14 to 15 minute duration. The fall-off in the number of events of longer duration suggests that this result is not very sensitive to the selection of 15 minutes as the upper limit on event duration. The results clearly are quite sensitive to the selection of 3 minutes for the lower limit on the event duration. The 4 to 5 minute bin contains 41 events making it the mode of this sample. However, the steep fall-off in the number of events as the duration is reduced (17 events in the 3 to 4 minute bin) suggests that the lower limit on event duration was fortuitously selected at an appropriate value.

Figure 3.5 The number of asteroid-like events of a given duration is plotted as a histogram versus the event duration. There is a maxima at 4 minutes duration and a steep fall-off towards shorter durations.
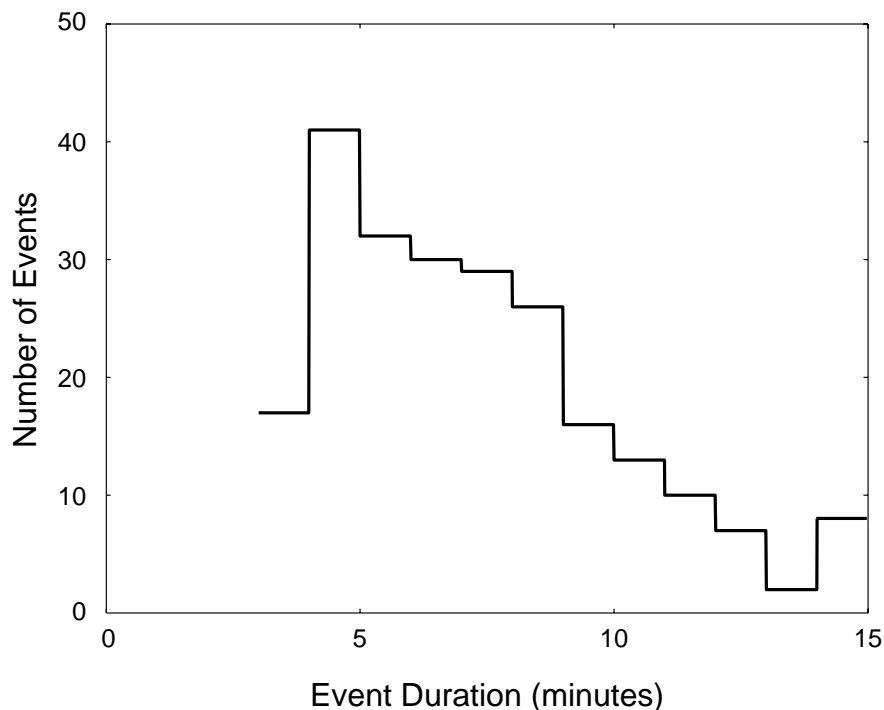
Although the events selected depend on the precise quantitative criteria imposed, the most significant filter in the asteroid-like event selection was the visual identification process. The selection criteria used in this study identified 231 asteroid-like events in 27 days of data. This contrasts with the 62 events identified in the initial visual inspection that was performed to help formulate the selection criteria (section 2.3). Obviously, the statistical results are subject to large uncertainty. However, the procedure has been designed at each step to bias the results towards overestimating the likelihood of observing asteroid-like events.

3.2 Analysis

In order to determine the probability of observing an event, the probability distribution function of the events must be determined. Selecting an appropriate distribution function requires both an understanding of the data and of the questions about the data that are to be answered. Some distribution functions are valid representations of the data only when events are random or independent of each other. Others require that the probability of observing an event be finite for all values of the independent parameter. For this study, a distribution function that is appropriate for determining the probability of observing an event in a given amount of time, and that does not assume that events are independent (non-clustered), is required.

3.2.1 Poisson Distribution

The Poisson distribution is commonly used to describe data from counting experiments where the data represent the number of observed events per unit time interval (Bevington, 1969). It is most commonly used to determine the probability that an event will occur within some time interval after the start of an experiment; other applications are also valid.

In order to satisfy a Poisson distribution, events must satisfy the following criteria:

1. The maximum number of events during a single time sample is 1
2. The number of events in the open interval (t, t+s) for s > 0 is independent of the number of events in the interval (0, t).
3. The number of events in the interval (t, t+s) depends only on s.

(Kaminsky and Rumpf, 1979). The first criterion is guaranteed to be satisfied by the event selection criterion that requires event separations to be at least 3 samples. The second criterion is satisfied if the distribution of events is independent of the interval over which events are identified (i.e. that the same distribution would be observed over different time intervals). Inspection of Figure 3.2 suggests that this condition is also met. If the data set had began on Feb 3 rather than Feb 1, 1991, and extended an additional two days, the distribution of asteroid-like events would remain mostly the same. The third criterion is a statement of stationarity (Kaminsky and Rumpf, 1979). If the average rate at which events are observed is not constant, then the number of events in the interval (t, t+s) will be functions of both t and s. The large

variance about the mean in the asteroid-like event occurrence rate suggests that this stationarity condition may not be met.

If all 3 criteria are met, then the Poisson probability (P_P) of observing x events in time interval t is

$$P_P(x, t, \tau) = e^{\frac{-t}{\tau}} \frac{1}{x!} (\frac{t}{\tau})^x \qquad (3.1)$$

where τ is a constant of proportionality that may be associated with the mean time between events (Bevington, 1969). If $\mu = \frac{t}{\tau}$ is the average number of events observed in time interval t, then

$$P_P(x, \mu) = \frac{\mu^x}{x!} e^{-\mu} \qquad (3.2)$$

where μ is the mean of the distribution. Bevington shows that the expectation value of x, $<x>$, is equal to the mean as follows:

$$<x> \quad = \sum_{x=0}^{\infty} (x \frac{\mu^x}{x!} e^{-\mu}) \quad = \mu e^{-\mu} \sum_{x=1}^{\infty} (\frac{\mu^{x-1}}{(x-1)!}) \quad = \mu e^{-\mu} \sum_{y=0}^{\infty} (\frac{\mu^y}{y!}) \quad = \mu$$

The Poisson distribution is parameterized by the single variable μ. It is not necessary to introduce the variance as a parameter since the variance and the mean are equal ($\sigma^2 = \mu$) in a Poisson distribution.

To compare the observed probability distribution of asteroid-like events in the solar wind with a Poisson distribution, the data must be organized by the temporal spacing between observed events. Figure 3.6 shows a histogram of the observed number of asteroid-like signatures, plotted versus the event separation time, where the data have been collected into twenty minute bins. Also shown in Figure 3.6 is a Poisson probability function for the sample mean occurrence rate of 2.68 hours (161 ± 17 minutes). Figure 3.6 clearly shows that the number of events observed at large separation times is much greater than the Poisson probability distribution function predicts. The sample variance is 4.31 hours which is not within the error of the sample mean as expected for a Poisson distribution.

In order to determine if the difference between the predicted Poisson probability of each observation bin and the actual binned observations is statistically reasonable, a (χ^2) test was performed. χ^2 measures the "goodness" of a fit between observations and a model by computing the sum of the squares of the deviations between the observations and predictions, weighted by the variances of the observations.

$$\chi^2 = \sum_{i=1}^{N} \frac{(y_i - y(x_i))^2}{\sigma_i^2} \qquad (3.3)$$

43

Figure 3.6 Histogram of the observed number of asteroid-like events in 20 minute bins plotted versus the event separation time. Also plotted is a Poisson distribution with the observed sample mean time between events of 161 minutes. The Poisson distribution fits the main peak of observed distribution fairly well but does not fit the tail of the distribution at large separation times.
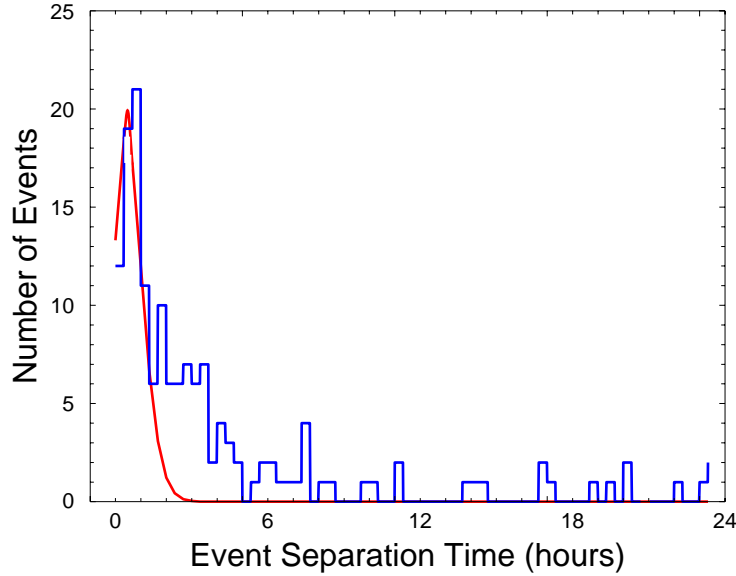
Since the variance of the observations is unknown, the observations are assumed to have a variance equal to the mean; an assumption that would be correct for a Poisson distribution. Hence,

$$\chi^2 = \sum_{i=1}^{N} \frac{(obs_i - predict_i)^2}{<obs>^2} \qquad (3.4)$$

The ratio of χ^2 to the number of degrees of freedom in the problem, known as the *reduced chi-square* χ_ν^2, is a good estimate of the probability that the appropriate fitting function has been selected (Bevington, 1969). The number of degrees of freedom (ν) in a sample of size N is $\nu = N - n - 1$ where n is the number of free parameters in the equation. There is only 1 free parameter μ in a Poisson distribution. $\chi_\nu^2 = 1$ indicates that there is an optimal fit. $\chi_\nu^2 < 1$ suggests an over estimate of the variances of the observations and $\chi_\nu^2 > 1.5$ indicates that an inappropriate fitting function has been selected (Bevington, 1969). The χ_ν^2 of the Poisson fit to the observations in Figure 3.6 is 1.87, indicating that the deviation from a Poisson distribution is statistically significant — that the Poisson distribution does not adequately describe the observations.

Despite the fact that the Poisson distribution does not fit the observations of DD many authors including Burlaga (1969) and Tsurutani and Smith (1979) have used this distribution to describe their data. Burlaga explains the observed clustering in the data as an expected result of an exponential distribution. There is no particular mention in this paper of the fit at large separation times nor whether or not the expected relationship between the variance and the

mean is observed. Tsurutani and Smith (1979) suggest that the poor fit to their events at large separation times might be an artifact of data gaps. The fact that the variance in the data cannot be reconciled with a Poisson distribution is cited as evidence that the ROID is non-stationary and changes with time. Since the occurrence rate of asteroid-like events does not fit a stationary Poisson distribution, other distribution functions are explored.

3.2.2 Lognormal Distribution

A positive random variable x is said to be lognormally distributed with two independent parameters μ and σ^2 if $Y = \ln(x)$ is normally distributed with mean μ and variance σ^2 (Shimizu and Crow, 1988). Lognormal distributions can be parameterized in other ways, with fewer or greater numbers of parameters, but the standard two parameter distribution is generally denoted by $\Lambda(\mu, \sigma^2)$ where the independent variable, x is not considered a parameter of the distribution. The probability density function, $P(x)$, for a distribution $\Lambda(\mu, \sigma^2)$ is

$$ P(x) = \frac{1}{\sqrt{2\pi}\sigma x} \exp\left(-\frac{(ln(x) - \mu)^2}{2\sigma^2}\right) \qquad for \quad x > 0 \qquad (3.5) $$

In the asteroid-like event data set, the independent variable (x) is the event separation time. If these data are lognormally distributed, then the number of observed events plotted versus the natural logarithm of the event separation times should be a Gaussian. Figure 3.7 shows a histogram of the number of asteroid-like events, in 4 equally spaced bins per decade, versus the natural logarithm of the event separation times. The dashed line is the lognormal distribution function $\Lambda(\mu = 4.36, \sigma^2 = 1.51)$ where 4.36 is the average of the natural logarithm of the event separation times and 1.51 is the variance about this average. The reduced chi-square X_ν^2, introduced in the last section, of the fit of this distribution to the observations is 1.03.

The moments of lognormal distribution function have some interesting properties, particularly when stated in terms of the independent variable x rather than $\ln(x)$. It can be shown that the expectation value of x, or $<x> = e^{\mu + \frac{\sigma^2}{2}}$ in following way:

$$ < x > = \int_0^{+\infty} x \, P(x) \, dx = \int_0^{+\infty} \frac{1}{\sqrt{2\pi}\sigma} \exp\left[-\frac{(ln\frac{x}{x_o})^2}{2\sigma^2}\right] dx \qquad (3.6) $$

where $\ln(x_o) = \mu$ Making the change of variable,

$$ y = ln(\frac{x}{x_o}), \qquad dy = \frac{1}{x}dx = \frac{dx}{x_o \, e^y} \qquad \Longrightarrow \qquad dx = x_o e^y dy $$

Figure 3.7 Histogram of the observed number of events (solid line) versus separation time (minutes) binned on a equally spaced natural logarithmic grid with 4 bins per decade. The dashed line is the predicted number of events determined by using the observed mean (μ) and variance (σ^2) of the log of the event separation times. The observed and predicted traces match quite well as indicated by a reduced X^2 value of approximately 1.
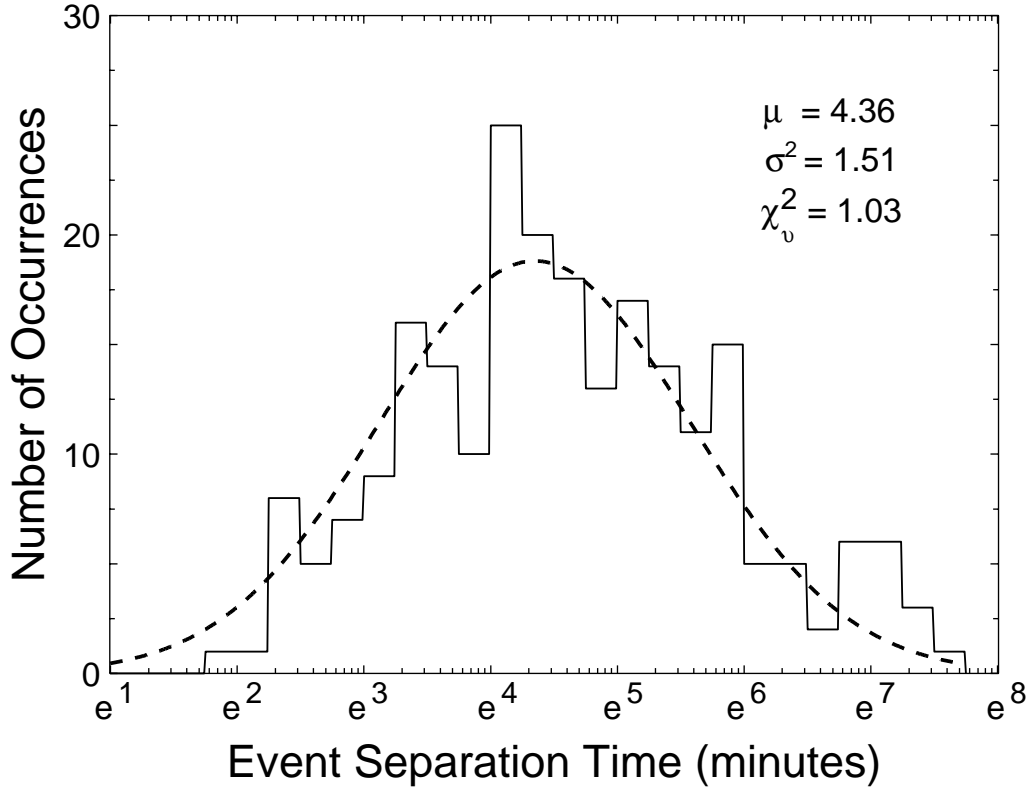
and the appropriate changes in the limits of integration we have

$$
\begin{aligned}
<x> &= \frac{x_o}{\sqrt{2\pi}\sigma} \int_{-\infty}^{+\infty} e^{-\frac{y^2}{2\sigma^2}} e^y \, dy \\
&= \frac{x_o}{\sqrt{2\pi}\sigma} e^{\frac{\sigma^2}{2}} \int_{-\infty}^{+\infty} \exp\left[\frac{-1}{2\sigma^2}(y^2 - 2\sigma^2 y + \sigma^4)\right] dy \\
&= \frac{x_o}{\sqrt{2\pi}\sigma} e^{\frac{\sigma^2}{2}} \int_{-\infty}^{+\infty} \exp\left[\frac{-1}{2\sigma^2}(y - \sigma^2)^2\right] dy \\
&= x_o e^{\frac{\sigma^2}{2}} \quad\quad\quad\quad\quad\quad\quad\quad\quad\quad\quad (3.7)
\end{aligned}
$$

$$
<x> = e^{(\mu + \frac{\sigma^2}{2})} \quad\quad\quad\quad\quad\quad\quad\quad\quad\quad\quad (3.8)
$$

The expected value of x is generally stated in the form of equation 3.8 (Shimizu, 1988). However, equation 3.7 more clearly demonstrates the interesting result – that the expected value of x is greater than the expected value of the lognormal distribution except when the variance is zero. Shimizu (1988) shows that $\text{Mode}(x) = e^{\mu - \sigma^2}$, $\text{Median}(x) = e^{\mu}$, and $<x> = e^{\mu + \frac{\sigma^2}{2}}$ or that $\text{Mode}(x)$

$\le$ Median(x) $\le$ Average(x). The moments of the lognormal distribution for the asteroid-like event data are: Mode = 18 minutes, Median = 78 minutes, and Average = 161 minutes. The higher order moments of this lognormal distribution are skew = $(w+2)(w-1)^{\frac{1}{2}} = 12.3$ and kurtosis = $w^4 + 2w^3 + 3w^2 - 3 = 664$ where $w = e^{\sigma^2}$.

Paquette (1972) observed that ocean current speed data were well described by a lognormal distribution, rather than an expected normal distribution, for several large, stable, current systems including the California Current. In this study, Paquette explains the lognormal distribution of current speed data, v, which is measured in units of Δv as an artifact of measuring the properties of a moving fluid with a stationary measuring device. A lognormal distribution describes his observations, $ln(v)$, in increments of $\Delta log(v)$. His argument is that except near zero, this is well approximated by $\frac{\Delta v}{v}$. Thus the original intervals are condensed in proportion to the speed in that interval, and the probability density is increased with proportion to v as a result. He then asserts that the observed lognormal distribution in time is approximately equivalent to a Gaussian distribution in a coordinate system that travels with the water parcel at varying speeds. The lognormal distribution in time is the result of a normal distribution in space, in the fluid parcel rest system. (Paquette, 1972).

This assertion by Paquette has interesting consequences for this study. The solar wind speed is so much greater than the speed of a spacecraft that the motion of the spacecraft can be ignored. Many authors have noted that DDs tend to cluster in regions of space associated with various solar wind structures including high speed streams (Belcher and Davis, 1971; Belcher and Solodyna, 1975; Saka and Kitamurta, 1976; Solodyna et al., 1977; Burlaga et al., 1977). The hypothesis that ROID, and the subset which are asteroid-like, are consistent with a simple, possibly Gaussian, spatial distribution of DDs convecting past an observing spacecraft at variable speeds is left to be tested at a future time. For now, the lognormal distribution provides the best characterization of both the mean and variance in the time ordered data. The lognormal distribution $\Lambda(\mu = 4.36, \sigma^2 = 1.51)$, whose parameters were derived from the data, will now be used to estimate the probability that the Galileo asteroid observations are random events in the solar wind.

3.2.3 Probability of Observing an Asteroid-Like Signature in the Solar Wind

In order to determine the likelihood that the field rotations near the asteroid flybys were random fluctuations in the solar wind, a time interval for observing such an event must be defined. We now define "a short interval of a flyby where an event associated with an asteroid could plausibly be located" as the 15 minute time interval centered at the time of a small asteroid closest approach. This definition is by no means rigorous. However, the rotations at both Gaspra and Ida meet this requirement and it is consistent the usage of 15 minute intervals elsewhere in this study. We will now consider how likely it is to observe an asteroid-like event in any 15 minute interval. We also compute the likelihood of observing only a single signature in the appropriate subinterval during a much longer observation.

Even though the lognormal distribution fits the observations exceptionally well, it does not allow us to directly compute the probability of observing a single event within a specific time interval after the start of the data set. The lognormal distribution describes the probability of observing a second event, in a given time interval, after having previously observed an event. For an arbitrarily selected time interval, where there is no knowledge of the field behavior prior to the interval, the probability of observing an event is the ratio of the interval duration to the average event frequency. Using 15 minutes for the interval duration and 161 minutes for the average event frequency, the probability of observing an asteroid like event is $\frac{15}{161} = 0.093 = 9.3\%$. Since the data are so highly skewed towards low separation times, this estimate is too low for an asteroid flyby on an "active" day when many events are occurring. On the other hand, there are many days in the study interval that have far fewer than the average number of events per day (hour, etc.). On one of these days, the average separation time gives too high an estimate of the probability of observing an asteroid-like signature in the absence of an asteroid.

There is, however, additional information in the distribution of events that can be used to provide insight as to the likelihood that the events observed during the Galileo asteroid flybys were random solar wind events. The event distribution is highly skewed and the events are clearly not randomly distributed in time. Figure 3.8 shows all of the observed asteroid-like events as individual points (plus signs) plotted as functions of time (horizontal axis) and day (vertical axis). The lightly shaded region between days 13 and 21 indicates an interval of several days where a higher than average number of events occurred. The darker shaded interval, days 17–19, contains the highest concentration of events in the dataset. Days 2–6 and 22–26 have lower than the average number of events. Figure 3.8 clearly illustrates that events cluster within the data set. Some days which have few or average numbers of events seem to have most of the events within a 6–7 hour interval (day 1, 06:00–13:00 UT), (day 19, 15:00–21:00 UT), (day 20, 11:00–17:00 UT). Other days with large number of events (10, 17, 18) have intervals of several hours where no events occur.

During the two Galileo asteroid flybys, nearly two hours of continuous high resolution data were acquired. In each of these intervals, one and only one asteroid-like event was observed, both near the center of the interval at closest approach. We can use this information to refine our probability analysis. Given an initial event, the lognormal probability density function can be used to determine the probability of observing a second event in any subsequent interval. Since the probability density function decreases for separation times greater than 17 minutes, the maximum probability that the Galileo events were random events is calculated by setting the time of the initial event just prior to the start of data acquisition. The probability density function is then integrated over the 15 minute interval at the center of a 2 hour data acquisition period. This gives[9]

$$P[52.5, 67.5] = \int_{52.5}^{67.5} \frac{1}{\sqrt{2\pi}1.23x} \exp\left[-\frac{(ln(x) - 4.36)^2}{2*1.23^2}\right] dx = 0.079.$$

---

[9]   This integrals was solved analytically and verified numerically.

Figure 3.8 Asteroid-like events are plotted as plus signs versus the time of day (horizontal axis) and day of month (vertical axis) where they occurred. Events appear to cluster with large time intervals with few events and short time intervals with many events. The lightly shaded region between days 13 and 21 indicates an interval of several days where a higher than average number of events occurred. The darker shaded interval, days 17–19, shows the highest concentration of events in the data set. Even in these high event concentration days, periods of several hours can be found where no events occur.
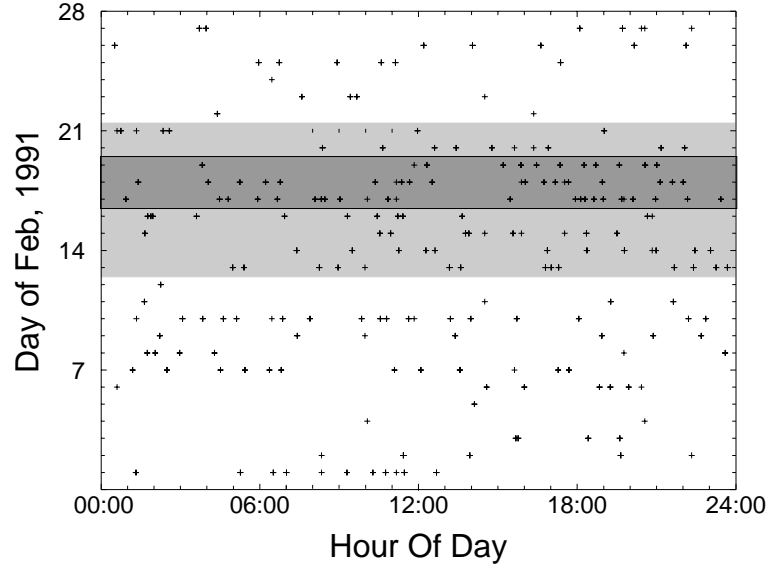
The probability of observing one event in a 15 minute interval after having not observed an event for at least 52.5 minutes is 7.9%. If the last event did not occur just before the start of the observation, then the probability is less than 7.9%. For instance, if the previous event occurred 45 minutes before the start of the observation, then probability of observing an event in the 15 minute window would be reduced in half. However, once an event has been detected, it can be used as a starting point for the determination of the probability of seeing another event in the remainder of the 2 hour interval. This probability is determined by integrating the probability density function over the time remaining in the interval (52.5 minutes).

$$P[0, 52.5] = \int_0^{52.5} \frac{1}{\sqrt{2\pi}1.23x} \exp\left[-\frac{(ln(x) - 4.36)^2}{2*1.23^2}\right] dx = 0.373.$$

The probability of not seeing an event in the remainder of the interval is therefore $1.0 - 0.373$ or 62.7%. The maximum probability that only one event is observed in the central 15 minutes of a 2 hour observation is the joint probability of both of these events occurring. The joint probability is the product of the two probabilities which is $0.079 * 0.627 = 0.050 = 5.0\%$ or one chance in twenty.

Another approach to quantifying the probability of observing a single event in the center of a two hour interval where the distribution of events over time is non-uniform is to remove event clusters and re-normalize the data set. The complete data set contains 231 events over 27 days (38880 minutes). Define an event cluster as any collection of events where the maximum spacing between intracluster events is less than or equal to two hours. Using this definition, 193

of 231 events are contained in 41 event clusters. The total time duration of all of the clusters is only 7631 minutes (5 days, 07:11). If all event clusters are removed from the data set, then the 38 remaining events are spread over 31241 minutes (21 days, 16:41). The average time between non-clustered events is 822 minutes. Using this average occurrence rate, the probability of observing only one event in a 2 hour window is $120/822$ or 14.6%. The probability that this event occurs in a particular 15 minute window is 1.8% or one chance in 55. This simple discussion of event clustering indicates that the previous estimate of the probability of observing a single event in a two hour interval (5.0 %) is likely to be an overestimate.

It is natural to ask what the likelihood of observing random asteroid-like signatures at two successive asteroid flybys. This would be the joint probability of observing two individual events which is the individual event probability squared. Values between 1:100 to 1:2500 are found. However, since the observed signature at Ida does not meet the selection criteria for asteroid-like events, this joint probability estimate is unjustified.

4 Summary and Conclusions

In Chapter 1, the Galileo magnetometer data in the vicinity of two asteroids was shown to have short duration, rotational perturbations at about the time the spacecraft crossed the interplanetary magnetic field line that passed through these asteroids. A theoretical basis for how these perturbations could be the result of an interaction between the IMF and the small bodies was also reviewed. Based on the work of Wang and Kivelson (1996) it was postulated that these perturbations could be the result of the spacecraft passing through a whistler wake of the asteroids. A whistler wake is produced by the flow of a magnetized plasma past a magnetized body whose scale size lies between the ion and electron gyroradii. The Gaspra event is quite dramatic and was quickly postulated to be the result of an asteroid-solar wind interaction. The perturbation near Ida is less dramatic, possibly because it occurs in a larger background field. However, the Ida signature occurs at the predicted location for a whistler wake signature during IMF conditions that were very different from the conditions when Galileo passed by Gaspra. The question was then posed, how likely is it that these perturbations are not associated with the presence of the nearby asteroid? What is the maximum occurrence rate of events similar to those observed during the Galileo asteroid flybys when no asteroid is present?

Having posed this question, the process by which signatures similar to those observed during the Galileo asteroid flyby could be identified in a solar wind magnetic field data set was described. The signatures observed at Gaspra and Ida were rotational with the IMF returning to its background orientation after only a few minutes. These characteristics were incorporated into a set of selection criteria that require that an event contain a rotational discontinuity and have a finite duration, where the duration was defined as the time to return to the background orientation. Several accepted IMF discontinuity detection criteria were considered as a potential starting point. The DD selection criteria put forth by Tsurutani and Smith (1979) were selected since these criteria tend to accept the greatest number of events. A less stringent set of RD identification criteria than those advocated by Neugebauer et al. (1984) were then adopted to ensure that the selected events would allow the maximum rate of occurrence to be estimated. The Ulysses magnetometer data acquired during the asteroid belt crossing was identified as the data set to search for asteroid-like signatures not associated with asteroid near-encounters. This data set was selected because magnetometer data were available at a high enough sampling rate to observe short duration perturbations. Since the solar wind ion and electron gyro radii vary with distance from the Sun, and their values control the scale lengths of IMF structures, only data sets acquired at radial distances of 2–3 AU were considered for this study.

After establishing the criteria by which asteroid-like events would be identified, the results and interpretation of the search for asteroid-like events in the Ulysses magnetometer data set were presented. First, the IMF conditions observed during the Ulysses crossing of the asteroid belt were shown to be similar to those observed by other spacecraft. Had the IMF conditions been anomalous, results from the analysis of this data set would not be applicable to other time

intervals or spacecraft observations. The Ulysses data set was shown to have an average of 8.96 asteroid-like events per day but the events were not uniformly distributed in time. The distribution of asteroid-like events was found to be well approximated by a two parameter lognormal distribution $\Lambda(\mu = 4.36, \sigma^2 = 1.51)$. Previous works on solar wind discontinuities have characterized the distribution of DDs as Poissonian and argued that the poor fit to the tail of the distribution at large event separation times was not important to the understanding of the problem (Burlaga 1966, Tsurutani and Smith 1979). In addition, the statistical result was shown to be fairly stable when selection criteria were adjusted slightly from those adopted for this study. The effects of event selection bias during periods of enhanced field strength appear to be small. The determination of whether or not the field returns to a background orientation provides the greatest statistical uncertainty in this result. This is based on a visual identification process that appears to be repeatable if not precise.

Based on this body of work, the following two conclusions can be reached: 1) The magnetic perturbation observed during the Gaspra flyby can be attributed to the presence of Gaspra with little uncertainty, and 2) the previous work on the occurrence rate of solar wind discontinuities (Siscoe et al., 1968; Burlaga 1969; Tsurutani and Smith, 1979) has not adequately characterized the nature of the distribution of these events.

It was argued that the probability of observing a single asteroid-like signature, in a 15 minute interval centered about closest approach to an asteroid within a two hours of continuous data, is 5%. The probability that the Gaspra signature is unrelated to the presence of the asteroid is likely to be substantially less. The 5% probability estimate assumes that an event occurred just prior to the start of the 2 hour observation of Gaspra. The distribution of asteroid-like signatures in the solar wind is non-uniform and highly clustered. In time intervals where only 1 event would be detected in a 2 hour observation, it is not likely that another event would have occurred just prior to the start of that observation. The average spacing between events separated by at least 2 hours is more than 13 hours. In addition, the distribution of asteroid-like events is derived from selection criteria which accept marginal events. A factor of 4 more events were selected by these criteria than were identified by a purely visual event selection procedure. The probability of observing a single event at the center of a 2 hour interval reported here is substantially overestimated by both the event selection criteria and the probability estimation method.

Furthermore, the field perturbation observed at Gaspra not only occurs in the appropriate interval near closest approach, it occurs at the time when the spacecraft reaches the spatial region accessible to whistler waves propagating away from the asteroid along IMF field lines. The perturbation orients the field lines in a manner that is consistent with the orientation expected from a whistler wake. It was impossible to add an event selection criterion to account for the combination of spacecraft location, IMF orientation, asteroid location, and perturbation direction required for a whistler wake crossing. The likelihood of observing a magnetic field perturbation of a particular shape and symmetry, at both a specified time and place, is less than one derived from only time and shape constraints. Taking all of these facts together, it can be stated with

confidence that this perturbation results from a solar wind — Gaspra interaction. The hypothesis that this perturbation is a random solar wind feature can be rigorously rejected at the 95% confidence level and can probably be rejected at the 99% confidence level.

The likelihood that the magnetic field perturbation observed near Ida is unrelated to the asteroid was not determined by this study. The selection criteria used to identify asteroid-like signatures do not accept small perturbations like the Ida signature. The Ida perturbation has the correct shape and symmetry for a whistler wake crossing. During the test for bias in the result against observing events in strong fields, alternative RD selection criteria were adopted. These alternative criteria allow small perturbations to be selected if they are substantially larger than other fluctuations about the mean in vicinity of the event. The Ida signature would be allowed by this set of selection criteria. This study does not suggest or imply that the field perturbation at Ida is unrelated to the asteroid.

The distribution of asteroid-like events is clearly not Poissonian. Neither the long tail on the distribution in the direction of distantly spaced events nor the variance of the number of events about the mean can be fit by using a Poisson distribution. Similar tails on the distribution of solar wind discontiniuties and large variances have been ignored by previous authors who have fit their data to a Poisson distribution (Burlaga, 1969; Tsurutani and Smith, 1979). Tsurutani and Smith suggest that the mean ROID is time variable or non-stationary and this accounts for the large variances observed. They argue further that, on average, the ROID fits a Poisson distribution. Clustering of directional discontinuities was first noted by Burlaga (1969) who explained it as an expected property of an exponential distribution. Burlaga and Davis (1971) and others (Belcher and Solodyna; 1975; Solodyna et al. 1977) later noted a relationship between high solar wind speed and disturbed fields and visa-versa. Belcher and Solodyna (1975) proposed that the short period "clumpiness" of the occurrence rate of these events is related to large scale structures such as Alfvén waves. We suggest that the analysis of the distribution of all DDs in the solar wind would be improved by considering the properties of the lognormal distribution.

4.1 Topics for Future Study

Additional insight into the distribution of solar wind discontinuities might be gained by testing the hypothesis that their distribution is better organized in spatial rather than temporal coordinates. Velocity aliasing effects on the distribution in time, such as the observed increase in ROID during periods of high solar wind speed (Belcher and Davis, 1971; Belcher and Solodyna; 1975; Solodyna et al. 1977) would be an expected result if the DDs are uniformly distributed in the plasma rest frame. Other aspects of the observed distribution in time, such as the association with large scale structures in the solar wind (Belcher and Solodyna, 1975; Solodyna et al., 1977) might be associated with a non-uniform distribution, or discontinuity propagation, in the plasma rest frame, while still reproducing the association with high flow speeds in the time domain. In the plasma rest frame, DD's are either stationary (contact, tangential) or propagate at the Alfvén speed (rotational), which is much less than the solar wind speed. Any corrections to

the spatial distribution for RD propagation effects should be small. Coleman (1967) presents a simple method for determining the propagation speed and direction of discontinuities in the solar wind rest frame.

Regardless of whether or not DD's have a simple distribution in the plasma rest frame, it is clear that the distribution of DDs in time is not well described by the Poisson distribution. Neither the high number of events that are observed at large separation times nor the variance about mean event separation time are consistent with a Poisson distribution. Unless the data can be shown to be in agreement with some other spatial distribution in the plasma rest frame, the time-series data are best interpreted through the use of the lognormal distribution. The lognormal distribution fits the tail and the peak of the observations, and the variance about the mean, without ignoring data at either end of the frequency spectrum.

It would be useful if the identification of asteroid-like like events could be done in a fully automated fashion. If the problem of eliminating step function discontinuities can be overcome, then a more objective measure of whether or not the field returns to an unperturbed state could be applied to the data. This would reduce the need for "generous" visual selection criteria that allow marginal events to be accepted. The formalization of event selection criteria into a computer algorithm would allow the verification of results by others. In addition, the statistical base of the study could be easily be expanded should high time resolution solar wind data become available from either of the Pioneer 10/11 spacecraft or some current/future mission such as NEAR, Cassini, or others.

The simulation results of Wang and Kivelson (1996) need to be explored in greater detail. In particular, the geometric effects produced by the spacecraft trajectory relative to the whistler wake need to be better understood. The simulations were run with input parameters selected to approximate conditions at the time of the Galileo asteroid encounters. Other solar wind conditions should be considered. The results of these analysis could be used to refine the range of possible signatures that are expected for whistler wake crossings. These results could in turn be used to improve the asteroid-like signature selection parameters. New selection criteria could be developed that do not require a conventionally defined rotational discontinuity as part of the signature. It was demonstrated that such criteria could be defined and that they produce remarkably an event distribution remarkably similar to the RD event distribution. Event selection criteria that select the Ida event would make it reasonable to compute the joint probability of observing random solar wind events at both asteroid flybys.

Appendix A Listing of Identified Asteroid-like Discontinuities

The following is a listing of all asteroid-like signatures identified in the Ulysses 12 magnetometer data set. The columns are the event time, defined as the time of the first rotational discontinuity in the signature, the event type (1=boxcar, 2=square wave, 3=rapid onset/gradual return, 4=gradual onset/rapid return) and the event duration, rounded to the even number of minutes.

```
Event Date/Time        Type   Duration
----------------------------------
1991-Feb-01 01:18:56    4     4
1991-Feb-01 05:15:44    3     6
1991-Feb-01 06:30:24    1    11
1991-Feb-01 08:20:16    3     8
1991-Feb-01 09:17:52    1     4
1991-Feb-01 10:16:32    1     3
1991-Feb-01 10:45:20    1     5
1991-Feb-01 11:09:52    1     6
1991-Feb-01 11:28:00    1     7
1991-Feb-01 12:40:32    4     4
1991-Feb-02 07:00:16    1     6
1991-Feb-02 11:25:52    1     9
1991-Feb-02 13:56:16    1    12
1991-Feb-02 19:38:40    4     9
1991-Feb-02 22:19:44    2     4
1991-Feb-03 08:20:16    1    15
1991-Feb-03 15:40:48    1     4
1991-Feb-03 18:25:04    2     8
1991-Feb-03 19:36:32    1     8
1991-Feb-04 15:46:08    1     8
1991-Feb-04 20:33:04    3     5
1991-Feb-05 10:03:44    3     4
1991-Feb-06 14:06:56    1     6
1991-Feb-06 14:34:40    4     7
1991-Feb-06 16:00:00    1    11
1991-Feb-06 18:50:40    1     4
1991-Feb-06 19:15:12    1     7
1991-Feb-06 19:56:48    4     3
1991-Feb-06 20:25:36    2    11
1991-Feb-07 00:36:16    1     4
1991-Feb-07 02:29:20    1    15
1991-Feb-07 04:30:56    1     5
1991-Feb-07 05:26:24    1     3
1991-Feb-07 06:21:52    1     8
1991-Feb-07 06:48:32    3     4
1991-Feb-07 09:26:24    0     0
1991-Feb-07 11:05:36    1     5
```

```
Event Date/Time        Type   Duration
-----------------------------------
1991-Feb-07 12:05:20    3     4
1991-Feb-07 13:33:52    3     3
1991-Feb-07 15:37:36    2    10
1991-Feb-07 17:16:48    4     4
1991-Feb-07 17:41:20    1     8
1991-Feb-08 01:11:28    1     5
1991-Feb-08 01:44:32    1     6
1991-Feb-08 02:02:40    1     6
1991-Feb-08 02:58:08    1     6
1991-Feb-08 19:46:08    1     7
1991-Feb-08 23:35:28    2     8
1991-Feb-09 04:17:04    2     4
1991-Feb-09 07:24:48    1     6
1991-Feb-09 09:58:24    1     8
1991-Feb-09 13:23:12    1     4
1991-Feb-09 18:56:00    1    10
1991-Feb-09 20:52:16    2     7
1991-Feb-09 22:41:04    1    11
1991-Feb-10 02:13:20    2     7
1991-Feb-10 03:04:32    1     8
1991-Feb-10 03:50:24    1     3
1991-Feb-10 04:37:20    1     8
1991-Feb-10 05:07:12    1    11
1991-Feb-10 06:27:12    3     7
1991-Feb-10 06:51:44    3    10
1991-Feb-10 07:53:36    2     5
1991-Feb-10 09:50:56    1    10
1991-Feb-10 10:33:36    1     7
1991-Feb-10 10:47:28    1     5
1991-Feb-10 11:37:36    3     5
1991-Feb-10 11:50:24    4     7
1991-Feb-10 13:12:32    1    12
1991-Feb-10 13:58:24    2     3
1991-Feb-10 15:42:56    2     7
1991-Feb-10 18:03:44    1     4
1991-Feb-10 22:12:16    1    10
1991-Feb-10 22:51:44    3    10
1991-Feb-10 23:54:40    3     7
1991-Feb-11 01:20:00    1     4
1991-Feb-11 01:38:08    3     4
1991-Feb-11 19:16:16    3     7
1991-Feb-11 21:38:08    1    11
1991-Feb-12 14:30:24    1     3
1991-Feb-13 02:15:28    3    12
1991-Feb-13 04:58:40    1     9
1991-Feb-13 05:24:16    1     9
1991-Feb-13 08:14:56    2     9
1991-Feb-13 08:57:36    3     7
1991-Feb-13 09:58:24    1     9
1991-Feb-13 13:10:24    1     6
1991-Feb-13 13:36:00    2     9
1991-Feb-13 16:48:00    1     7
```

```
Event Date/Time        Type   Duration
-----------------------------------
1991-Feb-13 17:00:48     4     3
1991-Feb-13 17:17:52     3     9
1991-Feb-13 21:40:16     2     7
1991-Feb-13 22:24:00     2    11
1991-Feb-13 23:15:12     1     4
1991-Feb-13 23:40:48     1     6
1991-Feb-14 00:02:08     1    10
1991-Feb-14 07:23:44     3     4
1991-Feb-14 11:15:12     1     4
1991-Feb-14 12:17:04     1     9
1991-Feb-14 12:37:20     1     4
1991-Feb-14 16:52:16     2     6
1991-Feb-14 18:21:52     3     4
1991-Feb-14 19:47:12     1     9
1991-Feb-14 20:50:08     2     6
1991-Feb-14 20:58:40     3     4
1991-Feb-14 22:27:12     1     8
1991-Feb-14 23:02:24     3    14
1991-Feb-14 23:54:40     4     6
1991-Feb-15 09:29:36     1     5
1991-Feb-15 10:32:32     1     8
1991-Feb-15 10:57:04     3     9
1991-Feb-15 13:46:40     1     8
1991-Feb-15 13:54:08     4    10
1991-Feb-15 14:30:24     1    10
1991-Feb-15 15:34:24     1     4
1991-Feb-15 15:53:36     4     4
1991-Feb-15 17:31:44     1     4
1991-Feb-15 18:20:48     2     5
1991-Feb-15 19:30:08     1     5
1991-Feb-16 01:39:12     1     9
1991-Feb-16 01:45:36     1     3
1991-Feb-16 01:53:04     2     8
1991-Feb-16 03:36:32     3     5
1991-Feb-16 06:56:00     3     6
1991-Feb-16 09:18:56     1     7
1991-Feb-16 10:26:08     1    14
1991-Feb-16 11:13:04     1     3
1991-Feb-16 11:24:48     1     3
1991-Feb-16 13:39:12     1     6
1991-Feb-16 20:39:28     3     7
1991-Feb-16 20:50:08     1    14
1991-Feb-17 01:57:20     3     8
1991-Feb-17 04:28:48     1     5
1991-Feb-17 04:48:00     1     8
1991-Feb-17 05:55:12     3    13
1991-Feb-17 06:40:00     3     7
1991-Feb-17 08:05:20     3     8
1991-Feb-17 08:19:12     2     6
1991-Feb-17 08:27:44     2     5
1991-Feb-17 09:01:52     4     7
```

```
Event Date/Time        Type   Duration
----------------------------------
1991-Feb-17 10:03:44    3     4
1991-Feb-17 10:50:40    2     7
1991-Feb-17 11:09:52    1     12
1991-Feb-17 15:28:00    3     8
1991-Feb-17 17:56:16    2     3
1991-Feb-17 18:08:00    2     6
1991-Feb-17 18:17:36    2     5
1991-Feb-17 18:37:52    1     3
1991-Feb-17 18:59:12    1     6
1991-Feb-17 19:40:48    2     3
1991-Feb-17 19:46:08    3     3
1991-Feb-17 20:06:24    2     4
1991-Feb-17 20:57:36    3     7
1991-Feb-17 22:10:08    1     5
1991-Feb-17 23:25:52    1     8
1991-Feb-18 00:56:32    1     4
1991-Feb-18 01:24:16    2     4
1991-Feb-18 04:03:12    3     8
1991-Feb-18 05:14:40    1     5
1991-Feb-18 06:13:20    2     11
1991-Feb-18 06:46:24    2     6
1991-Feb-18 11:09:52    3     6
1991-Feb-18 11:21:36    3     6
1991-Feb-18 11:39:44    3     5
1991-Feb-18 12:30:56    1     13
1991-Feb-18 15:53:36    2     8
1991-Feb-18 16:02:08    3     5
1991-Feb-18 16:44:48    2     7
1991-Feb-18 17:10:24    3     5
1991-Feb-18 17:31:44    3     4
1991-Feb-18 17:40:16    1     4
1991-Feb-18 18:57:04    3     7
1991-Feb-18 21:08:16    1     6
1991-Feb-18 21:36:00    1     5
1991-Feb-18 22:00:32    1     5
1991-Feb-19 10:21:52    4     6
1991-Feb-19 11:50:24    2     8
1991-Feb-19 12:19:12    4     3
1991-Feb-19 15:12:00    1     7
1991-Feb-19 15:52:32    3     4
1991-Feb-19 16:27:44    2     8
1991-Feb-19 17:21:04    2     6
1991-Feb-19 18:15:28    4     12
1991-Feb-19 18:42:08    2     7
1991-Feb-19 19:35:28    2     9
1991-Feb-19 20:34:08    3     5
1991-Feb-19 21:00:48    3     6
1991-Feb-20 03:49:20    1     6
1991-Feb-20 08:22:24    2     5
1991-Feb-20 10:38:56    4     4
1991-Feb-20 12:36:16    1     4
1991-Feb-20 13:25:20    4     4
```

58

```
Event Date/Time        Type   Duration
----------------------------------------
1991-Feb-20 14:46:24     2     6
1991-Feb-20 15:37:36     3     7
1991-Feb-20 16:21:20     2     5
1991-Feb-20 16:54:24     3    10
1991-Feb-20 21:10:24     4     6
1991-Feb-20 22:03:44     1    10
1991-Feb-21 00:01:04     3     5
1991-Feb-21 00:36:16     3    11
1991-Feb-21 00:44:48     1     7
1991-Feb-21 01:20:00     1     9
1991-Feb-21 02:20:48     1     4
1991-Feb-21 02:34:40     1     4
1991-Feb-21 19:01:20     3    10
1991-Feb-22 11:57:52     3    12
1991-Feb-22 16:21:20     1     6
1991-Feb-23 04:23:28     3     8
1991-Feb-23 09:25:20     2    10
1991-Feb-23 09:40:16     4     3
1991-Feb-23 14:30:24     3     5
1991-Feb-24 07:35:28     1     4
1991-Feb-25 06:27:12     4     4
1991-Feb-25 06:44:16     1     6
1991-Feb-25 08:55:28     2     5
1991-Feb-25 10:35:44     1     8
1991-Feb-25 11:07:44     2    14
1991-Feb-25 17:22:08     1     4
1991-Feb-26 05:57:20     3     5
1991-Feb-26 12:11:44     1     5
1991-Feb-26 14:02:40     3     7
1991-Feb-26 16:37:20     3     8
1991-Feb-26 20:09:36     3    15
1991-Feb-26 22:06:56     1    15
1991-Feb-27 00:30:56     1     9
1991-Feb-27 03:42:56     3     5
1991-Feb-27 03:57:52     2     7
1991-Feb-27 18:05:52     1    11
1991-Feb-27 19:42:56     1    12
1991-Feb-27 20:25:36     4     5
1991-Feb-27 20:33:04     1     4
1991-Feb-27 22:19:44     2     9
```

Appendix B Variation of Statistical Parameters

Numerous parameters are involved in the automated selection of rotational discontinuities in this study. This appendix describes how values selected for those parameters determines the number of discontinuities that are then visually inspected to see if they are "asteroid-like".

Parameter Definitions

1. N: N is a "thickness" parameter, it is the number of records between samples that are differenced when determining ΔB, i.e. $\Delta B = B_i - B_{i-N}$. The nominal value of N is 3.
2. D: D is one of the variance parameters, it is the number of records used in the computation of δ where δ^2 is the larger of

$$\frac{1}{D} \sum_{i=t-N}^{t-(D-1)-N} |B_i - B_{i-1}|^2$$

and

$$\frac{1}{D} \sum_{i=t}^{t+(D-1)} |B_{i+1} - B_i|^2$$

The nominal value of D is 5.
3. S: S is the separation parameter, it is minimum number of records that can separate rotational discontinuities. If a second discontinuity is detected in S or fewer records, both discontinuities are disallowed. In this study, S was always set equal to 3 (nominal value of N) and not varied.
4. B_L is the larger of $|B_i|$ and $|B_{i-N}|$
5. dB_ratio: The dB_ratio is the size parameter which sets the minimum value of the ratio $\frac{|\Delta B|}{B_L}$ that is considered a potential discontinuity. The nominal value of dB_ratio is 0.5
6. δ_ratio: The δ_ratio is another variance parameter that defines the minimum value of the ratio $\frac{|\Delta B|}{\delta}$ where δ is the local variance. The nominal value of δ_ratio is 2.0
7. Eigenvalue ratio: The eigenvalue ratio is the ratio $\frac{\lambda_2}{\lambda_3}$ where the λ are the eigenvalues associated with the intermediate and minimum eigenvectors from the minimum variance analysis. The minimum eigenvalue ratio was set at 2 and not varied in this study.
8. Bn_ratio: The Bn_ratio is the minimum value of the ratio $\frac{B_n}{B_L}$ where B_n is the component of B that is normal to the discontinuity. The nominal value of the Bn_ratio is 0.2.
9. dB_ratio: The dB_ratio is the size of the change in the field magnitude across a discontinuity as measured by the ratio $\frac{\Delta |B|}{B_L}$. The nominal value of dB_ratio is 0.2

A single parameter is adjusted from its nominal value in each of the following subsections. Each subsection contains a table that summarizes how varying that single parameter impacts the number of rotational discontinuities (RDs) that are selected. The value of the parameter that is being varied is listed in the first column under the heading **value**. The result obtained when the nominal value of the parameter is used in the test is indicated by a row of values in boldface type. Identification of RDs is performed step-wise. First $\Delta\mathbf{B}$ is computed for a given N value, and then checked against the d**B**_ratio parameter. If the value of the ratio exceeds the value of the d**B**_ratio parameter, a potential event is identified. The number of potential events is the second column in the table. Next δ is computed in the vicinity of each potential event. The number of potential events excluded by this test is indicated in column 3 (**delta ratio**). Next, events are checked against the event separation parameter S. The number of events excluded by this test are indicated in column 4 (**S**). The events that remain have satisfied the Tsurutani and Smith (1979) selection criteria for solar wind discontinuities. These events are further tested to see if they qualify as rotational discontinuities. A minimum variance analysis is performed using 13 data points across the discontinuity. The ratio of the intermediate to minimum eigenvalues is used to determine if this structure is acceptably planar with a well defined minimum variance direction. The number of events that are excluded because the minimum variance direction is poorly defined are listed in column 5 (**lambda ratio**). If an event has a well defined minimum variance direction, in order to qualify as a rotational discontinuity, it must have a finite component normal to the discontinuity surface and must have a small change in field magnitude across that surface. The number of events that are excluded on the basis of the relative size of the normal component are listed in column 6 (**Bn ratio**). Column 7 (**dB ratio**) gives the number of events eliminated because the field magnitude changes too much across the discontinuity to be an RD. Finally, the number of **RDs** identified is listed in column 8.

Variation of N: Discontinuity thickness parameter

Table B.1 Variation of N

value	Potential Events	delta ratio	S	lambda ratio	Bn ratio	dB ratio	RD's
1	975	501	35	53	105	18	263
2	2315	850	536	103	201	24	601
3	**3554**	**1204**	**1233**	**127**	**257**	**47**	**686**
4	4556	1557	1855	130	248	38	728
5	5481	1823	2458	136	260	52	752
10	9230	2674	5103	119	309	57	968

When N is varied, the number of potential events changes considerably but the number of RD's changes little. The number of potential events increases as a result of accepting thick

discontinuities. The effect on the RD rate is offset primarily by the separation parameter S, which removes multiple counting of thick events. The other parameters simply respond to the increased number of potential events and increase roughly proportionally. The opposite effect is observed when N is reduced and only thin discontinuities are allowed.

Variation of the ratio |dB| to B, discontinuity size parameter

Table B.2 Variation of $\frac{\Delta B}{B}$

value	Potential Events	delta ratio	S	lambda ratio	Bn ratio	dB ratio	RD's
0.1	51946	18274	24402	572	2113	43	6542
0.3	9946	3465	3723	215	634	55	1854
0.4	5648	1980	2026	174	385	51	1032
0.50	**3554**	**1204**	**1233**	**127**	**257**	**47**	**686**
0.6	2283	784	754	91	169	35	450
0.7	1558	547	499	72	110	31	299
1.0	525	216	147	15	40	19	88

Clearly the number of potential events is highly dependent on how large a fluctuation is considered as a potential discontinuity. The smaller the allowed percentage variation across potential discontinuities, the more events are identified. The remaining event filters respond to the increased number of events by passing roughly the same proportion of potential events through the process. This tells us that the results are particularly sensitive to this parameter since there are no processes that moderate its effects.

Variation of D: the number of points included in the computation of data variance near a discontinuity

Table B.3 Variation of D

value	Potential Events	delta ratio	S	lambda ratio	Bn ratio	dB ratio	RD's
3	3554	1699	862	123	225	33	612
4	3554	1430	1094	125	228	33	644
5	**3554**	**1204**	**1233**	**127**	**257**	**47**	**686**
6	3554	1095	1342	140	244	41	692
7	3554	995	1449	136	244	40	700
15	3554	583	1783	136	254	42	756

Potential events are determined by the combination of the two previously described parameters. The number of points included during the computation of the local variance depends weakly on the number of RDs. The variance parameter and separation parameters appear to work in opposition to each other. When the number of points included in the variance calculation is decreased, the number of potential events that are removed by the variance filter increases and visa-versa. The separation parameter responds to the increase or decrease in the number of potential events that it has to act upon in such a way that nearly a constant number of events is passed to the other filters. The net result is that the two filters are not independent and this result is not very sensitive to variation in only one of the parameters.

Variation of dB to delta ratio, the data variance parameter

Table B.4 Variation of $\frac{|\Delta B|}{\delta}$

value	Potential Events	delta ratio	S	lambda ratio	Bn ratio	dB ratio	RD's
1	3554	567	1978	139	294	52	818
1.5	3554	778	1545	135	285	47	764
1.75	3554	1009	1366	136	277	45	721
2	**3554**	**1204**	**1233**	**127**	**257**	**47**	**686**
2.25	3554	1430	1063	117	239	43	652
2.5	3554	1617	957	112	228	36	604
4	3554	2583	342	68	137	22	402

The interdependence of the variance parameter (delta ratio) and the separation parameter (S) is evident again. When the delta ratio ($\frac{|\Delta \mathbf{B}|}{\delta}$) is relaxed, more events are passed to the separation parameter where they are filtered. As the delta ratio is increased, fewer events are available to the separation parameter filter and it removes fewer. The total variation in the number of RD's is fairly small, although somewhat larger than the variation observed when D was varied.

Variation of the Bn to B ratio, the normal component size parameter.

Table B.5 Variation of $\frac{B_n}{B}$

value	Potential Events	delta ratio	S	lambda ratio	Bn ratio	dB ratio	RD's
0.15	3554	1204	1233	127	182	45	763
0.2	**3554**	**1204**	**1233**	**127**	**257**	**47**	**686**
0.25	3554	1204	1233	127	297	37	636
0.3	3554	1204	1233	127	351	33	556
0.4	3554	1204	1233	127	487	26	477
0.5	3554	1204	1233	127	557	20	413

The minimum Bn ratio ($\frac{B_n}{B}$) necessary to qualify as a rotational discontinuity in the Neugebauer et al. (1984) classification of discontinuities was 0.4. However, the Neugebauer study contained a category of discontinuities that might be either rotational or tangential. The nominal value of 0.2 was selected in order to capture a significant fraction of the "either" events into the rotational classification. The number of potential events that are removed when this filter is tightened increases. The number of potential events available to this filter is low and the variation in number of RD's identified is moderate or high which indicates that the result is fairly sensitive to this parameter. However, by setting this value towards the low end of the scale, the requirement that events be clearly rotational in character is reduced as desired.

Variation of the ratio of d|B| to B, the field magnitude change parameter

Table B.6 Variation of $\frac{\Delta|\mathbf{B}|}{B}$

value	Potential Events	delta ratio	S	lambda ratio	Bn ratio	dB ratio	RD's
0.05	3554	1204	1233	127	257	184	549
0.10	3554	1204	1233	127	257	94	639
0.15	3554	1204	1233	127	257	65	668
0.2	**3554**	**1204**	**1233**	**127**	**257**	**47**	**686**
0.25	3554	1204	1233	127	257	39	694
0.3	3554	1204	1233	127	257	26	707
0.4	3554	1204	1233	127	257	18	715

The change in field magnitude across a purely rotational discontinuity should be zero. The same can be said about whistler waves propagating purely along the field lines. However, some compressional components are expected in "real" RD's and whistler waves are not required to propagate purely along field lines. The Neugebauer et al. (1984) discontinuity classification study placed the limit on this ratio at 0.2 and that value was selected as the nominal value in this study. Variation of this parameter by factors of 2 yields 8% changes in the number of RD's identified. This is partly the result of the effectiveness of the filters that are applied earlier in the process. The net effect however is to reduce the sensitivity of the result to the value of this parameter.

Appendix C Usage of the *discontinuity* **software**

The discontinuity identification software is not a stand alone program. It is an application or *fitting* within the I.G.P.P. Data Flow System (DFS). The DFS is a tool that allows the transfer of data between independent applications. Each application within the DFS uses a standard set of input and output operations that allow the code to extract data columns from the flow, manipulate the data, and pass the data downstream where other applications may act upon the data. The purpose of this section is to describe what combination of data columns must be available in the flow at the time this fitting is activated, the options that can effect the actions of the fitting, and the output of the fitting for all valid combinations of user options.

Input: required data columns

Time: A binary time column (seconds after a reference epoch) must be present in the flow, the name of the column can be specified by the user.

Magnetic field vector and magnitude: Three components of a magnetic field vector plus the field magnitude must be present in the flow. The fitting expects the data to be in RTN coordinates but this is not an absolute requirement for all permutations of user options (see options descriptions for details).

User options — (none required)   The following parameter specification conventions are used here:

Italics indicate a list of valid parameters for an option
Bold-face type indicates a default value
<> indicates units

TIME_COL: the name of the binary time column <seconds> (**time**)
B_COL: A comma separated list of 4 column names for the columns Br, Bt, Bn, |B| or equivalent (**Br,Bt,Bn,Bmag**).
METHOD: The discontinuity selection criteria to be used in the discontinuity identification process. The allowable values are **TSURUTANI**, NEUGEBAUER, MARIANI, and BURLAGA. Both the MARIANI and the BURLAGA selection criteria require input data in RTN coordinates. The TSURUTANI and NEUGEBAUER criteria can be applied to data in any coordinate system. However, the output columns lambda and delta should be disregarded if the input data are not in RTN coordinates.
LENGTH: The number of records between samples (N) that are compared in the computation of differences in the TSURUTANI and NEUGEBAUER selection criteria (**3**).
DISTANCE: The number of records used in the computation of variance (D) in the TSURUTANI and NEUGEBAUER selection criteria (**5**).

DB_FACTOR: The minimum value of the ratio d**B**/B for the TSURUTANI and NEUGE-BAUER selection criteria (**0.5**).

SIGMA_FACTOR: The minimum value of the ratio d**B**/delta for the TSURUTANI and NEUGEBAUER selection criteria (**2.0**).

NORMAL_RATIO: The minimum value of the ratio Bn/B for the NEUGEBAUER selection criteria (**0.2**).

DBMAG_FACTOR: The minimum value of the ratio dB/B for the NEUGEBAUER selection criteria (**0.2**).

SAMPLE_RATE: The sample rate <seconds> of the input data (**12.0**)

MIN_DURATION: The minimum allowable time <seconds> between successive rotations in the TSURUTANI and NEUGEBAUER selection criteria (**36.0**).

BUFFSIZE: The maximum number of records in a buffer (**10000**). This application buffers data records and comparisons are only done within a single buffer.

Output   The exact output and the meaning of the output depends on the discontinuity selection criteria option. In all instances, the integer value 1 in the output column *rot* indicates a discontinuity has been identified at that record. The Neugebauer selection criteria identifies rotational discontinuities given a directional discontinuity has already been identified by the Tsurutani method. The two methods have identical output except that for value of *rot*. Values of *rot* other than 0 and 1 are used to identify which selection criteria was violated after an event has initially been identified as a potential discontinuity. Since there are additional Neugebauer constraints, *rot* can take on additional values.

Common Output:

   rot:

   > 0: No discontinuity identified
   > 1: A discontinuity has been identified at this record

   dB <nT>: The magnitude of the vector change between values separated by LENGTH records.
   dBmag <nT>: The difference in field magnitude vectors separated by LENGTH records.
   lambda <radians>: π – atan2(Bt, -Br)
   delta <radians>: asin(Bn/Bmag)

Tsurutani Selection criteria output:

   rot:

   > 2: The variance selection criteria was violated
   > 3: The separation selection criteria was violated

   sigma <nT>: The maximum variance over DISTANCE records on either side of the current record.

Neugebauer Selection Criteria Output:

rot:

2: The variance selection criteria was violated
3: The separation selection criteria was violated
4: The eigenvalue ratio was too small
5: The normal component was too small
6: The field magnitude change was too large

sigma <nT>: The maximum variance over DISTANCE records on either side of the current record.
l23ratio: Eigenvalue ratio
Bnratio: The ratio of Bn to B.

Burlaga Selection Criteria Output:

omega <degrees>: the angle through which the field rotates across a discontinuity as computed by Burlaga.

Mariani Selection Criteria Output:

theta <degrees>: the angle through which the field rotates across a discontinuity as computed by Mariani.

References

Alfvén, H., Existence of electromagnetic-hydrodynamic waves, *Nature*, 150, 405, 1942.

Balogh, A., T. J. Beek, R. J. Forsyth, P. C. Hedgecock, R. J. Marquedant, E. J. Smith, D. J. Southwood, and B. T. Tsurutani, The magnetic field investigation on the Ulysses mission: Instrumentation and preliminary scientific results, *Astronomy and Astrophysics Supplement Series*, 92, 2, 221, 1992

Belcher, J. W., and C. V. Solodyna, Alfvén waves and directional discontinuities in the interplanetary medium, *J. Geophys. Res.*, 80, 181, 1975.

Belton, M. J. S., J. Veverka, P. Thomas, P. Helfenstein, D. Simonelli, C. Chapman, M. E. Davies, R. Greeley, R. Greenberg, J. Heed, S. Merchie, K. Klaasen, T. V. Johnson, A. McEwen, D. Morrison, G. Neukum, F. Fanale, C. Anger, M. Carr, C. Pilcher, Galileo encounter with 951 Gaspra: First pictures of an asteroid, *Science*, 257, 1647, 1992.

Belton, M. J. S., C. R. Chapman, P. C. Thomas, M. E. Davies, R. Greenberg, K. Klaasen, D. Byrnes, L. D'Amaro, S. Synnott, T. V. Johnson, A. McEwen, W. J. Merline, D. R. Davis, J. M. Petit, A. Storrs, J. Veverka, and B. Zellner, Bulk density of asteroid 243 Ida from the orbit of its satellite Dactyl, *Nature*, 374, 785–788, 1995.

Bevington, P. R, *Data Reduction and Error Analysis for the Physical Sciences*, McGraw-Hill Book Co., New York, 1969.

Burgess, D., Collisionless shocks, in *Introduction to Space Physics* (edited by Kivelson and Russell), Cambridge Univ. Press, 1995.

Burlaga, L. F., Micro-scale structures in the interplanetary medium, *Solar Phys.*, 4, 67, 1968.

Burlaga, L. F., Large velocity discontinuities in the solar wind, *Solar Phys.*, 7, 54, 1969.

Burlaga, L. F., J. F. Lemaire, J. M. Turner, Interplanetary current sheets at 1 AU, *J. Geophys. Res.*, 82, 3191, 1977.

Burlaga, L. F., *Interplanetary Magnetohydrodynamics*, Oxford Univ. Press, New York, 1995.

Cohen, R. H., and R. M. Kulsrud, Nonlinear evolution of parallel-propagating hydro-magnetic waves, *J. Geophys. Res.*, 17, 2215, 1974.

Greenstadt, E. W., Conditions for magnetic interaction of asteroids with the solar wind, *Icarus*, 14, 374, 1971a.

Greenstadt, E. W., Possible magnetic interaction of asteroids with the solar wind, *Physical Studies of the Minor Planets*, proceedings of the 12th colloquium of Icarus, editor T. Gehrels, NASA SP-267, 567, 1971b.

Hudson, P. D., Discontinuities in an anisotropic plasma and their identification in the solar wind, *Planet. and Space Sci.*, 18, 1161, 1970.

Hundhausen, A. J., The Solar Wind, in *Introduction to Space Physics*, (edited by Kivelson and Russell), Cambridge Univ. Press, 1995.

Kaminsky, F. C., D. L. Rumpf, Simulating nonstationary Poisson processes: a comparison of alternatives including the correct approach, *Simulations*, 1, 17, 1977.

King, T. A., R. J. Walker, R. L. McPherron, and N. E. Cline, Data analysis by using parallel tasking and a data flow model (Abstract), *Eos Trans. AGU*, 69, 16, 410, 1988. Presented at the Spring AGU meeting, Baltimore, MD, 1988.

Kivelson, M. G., K. K. Khurana, J. D. Means, C. T. Russell, and R. C. Snare, The Galileo magnetic field investigation, *Space Sci. Rev.*, 60, 357, 1992.

Kivelson, M. G., L. F. Bargatze, K. K. Khurana, D. J. Southwood, R. J. Walker, and P. J. Coleman, Magnetic field signatures near Galileo's closest approach to Gaspra, *Science*, 261, 331, 1993.

Kivelson, M. G., Z. Wang, S. Joy, K. K. Khurana, C. Polanskey, D. J. Southwood, and R. J. Walker, Solar wind interaction with small bodies: 2. What can Galileo's detection of magnetic rotations tell us about Gaspra and Ida, *Adv. Space Res.*, 16, 459, 1995.

Krauss-Varban, D., Structure and length scales of rotational discontinuities, *J. Geophys. Res.*, 98, 3907, 1993.

Lepping, R. P. and K. W. Behannon, Magnetic field directional discontinuities, 1. Minimum variance errors, *J. Geophys. Res.*, 85, 4695, 1980.

Lepping, R. P. and K. W. Behannon, Magnetic field directional discontinuities, Characteristics between 0.46 and 1.0 AU, *J. Geophys. Res.*, 91, 8725, 1986.

Mariani, F., B. Bavassano, U. Villante, and N. F. Ness, Variations in the occurrence rate of discontinuities in the interplanetary magnetic field, *J. Geophys. Res.*, 78, 3191, 1977.

Neugebauer, M., D. R. Clay, B. E. Goldstein, and B. T. Tsurutani, A reexamination of rotational and tangential discontinuities in the solar wind, *J. Geophys. Res.*, 89, 5395, 1984.

Neugebauer M., and B. Buti, A search for evidence of the evolution of rotational discontinuities in the solar wind from nonlinear Alfvén waves, *J. Geophys. Res.*, 95, 13–20, 1990.

Neugebauer M., and C. J. Alexander, Shuffling foot points and magnetohydrodynamic discontinuities in the solar wind, *J. Geophys. Res.*, 96, 9409, 1991.

Neugebauer, M., D. R. Clay, J. T. Gosling, The origins of planar magnetic structures in the solar wind, *J. Geophys. Res.*, 98, 9383, 1993.

Paquette, R. G., Some statistical properties of ocean currents, *Ocean Engng,* 2, 95, 1972.

Russell, C. T. A brief history of solar-terrestial physics, in *Introduction to Space Physics* (edited by Kivelson and Russell), Cambridge Univ. Press, 1995.

Sari, J. W., Modulation of low energy cosmic rays, Ph.D. thesis, Univ. of Maryland, College Park, 1972. (Also available as document X-692–72–309, NASA Goddard Space Flight Center, Greenbelt, MD., Aug. 1972.)

Saka, O., and T. I. Kitamura, Further investigation on distributions of tangential discontinuity in the solar wind, *Planet. Space Sci.*, 24, 1043, 1976.

Shimizu, K., Point estimation, in *Lognormal Distributions*, (edited by Crow and Shimizu), Marcel Decker Inc, New York, 1988.

Shimizu, K. and E. Crow, History, genesis, and properties, in *Lognormal Distributions*, (edited by Crow and Shimizu), Marcel Decker Inc, New York, 1988.

Siscoe, G. L., L. Davis, P. J. Coleman, Jr., E. J. Smith, and D. C. Jones, Power Spectra and discontinuities of the interplanetary magnetic field: Mariner 4, *J. Geophys. Res.*, 73, 61, 1968.

Smith, E. J., Interplanetary magnetic field over two solar cycles and out to 20 AU, *Adv. Space Res.*, 9, 159, 1989.

Solodyna, C. V., J. W. Sari, and J. W. Belcher, Plasma field characteristics of directional discontinuities in the interplanetary medium, *J. Geophys. Res.*, 82, 10, 1977.

Tsurutani, B. T., and E. J. Smith, Interplanetary discontinuities: Temporal variations and the radial gradient from 1 to 8.5 AU, *J. Geophys. Res.*, 84, 2773, 1979.

Tsurutani, B. T., C. M. Ho, E. J. Smith, M. Neugebauer, B. E. Goldstein, J. S. Mok, J. K. Arballo, A. Balogh, D. J. Southwood, W. C. Feldman, The relationship between interplanetary discontinuities and Alfvén waves: Ulysses observations, *Geophys. Res. Lett.*, 21, 2267, 1994.

Tsurutani, B. T., C. M. Ho, J. K. Arballo, E. J. Smith, B. E. Goldstein, M. Neugebauer, A. Balogh, and, W. C. Feldman, Interplanetary discontinuities and Alfvén waves at high heliographic latitude: Ulysses, *Geophys. Res. Lett.*, 21, 2267, 1994.

Wang, Z., M. G. Kivelson, S. Joy, K. K. Khurana, C. Polanskey, D. J. Southwood, and R. J. Walker, Solar wind interaction with small bodies: 1. Whistler wing signatures near Galileo's closest approach to Gaspra and Ida, *Adv. Space Res.*, 16, 459, 1995.

Wang, Z. and M. G. Kivelson, Asteroid interaction with solar wind, *J. Geophys. Res.*, 101, 24479, 1996.